The Local Lyα Forest. III. Relationship between Lyα Absorbers and Galaxies, Voids and Superclusters [1]

Steven V. Penton, John T. Stocke, and J. Michael Shull [2]

Center for Astrophysics and Space Astronomy, Department of Astrophysical and Planetary Sciences, University of Colorado, Boulder CO, 80309

ABSTRACT

In this paper, we use large-angle, nearby galaxy redshift surveys to investigate the relationship between the 81 low-redshift Lyα absorbers in our HST/GHRS survey and galaxies, superclusters, and voids. In a subsample of 46 Lyα absorbers located in regions where the February 8, 2000 CfA catalog is complete down to at least L^* galaxies, the nearest galaxy neighbors range from $100h_{70}^{-1}$ kpc to $> 10h_{70}^{-1}$ Mpc. Of these 46 absorbers, 8 are found in galaxy voids. After correcting for pathlength and sensitivity, we find that $22 \pm 8\%$ of the Lyα absorbers lie in voids, which requires that at least some low-column density absorbers are not extended halos of individual bright galaxies. The number density of these clouds yields a baryon fraction of $4.5 \pm 1.5\%$ in voids.

The stronger Lyα absorbers ($10^{13.2-15.4}$ cm^{-2}) cluster with galaxies more weakly than galaxies cluster with each other, while the weaker absorbers ($10^{12.4-13.2}$ cm^{-2}) are more randomly distributed. The median distance from a low-z Lyα absorber in our sample to its nearest galaxy neighbor ($\sim 500h_{70}^{-1}$ kpc) is twice the median distance between bright galaxies in the same survey volume. This makes any purposed "association" between these Lyα absorbers and individual galaxies problematic. The suggested correlation between Lyα absorber equivalent width ($\mathcal{W}$) and nearest-galaxy impact parameter does not extend to $\mathcal{W} \leq 200$ mÅ, or to impact parameters $> 200h_{70}^{-1}$ kpc. Instead, we find statistical support for the contention that absorbers align with large-scale filaments of galaxies. The pair of sightlines, 3C 273 and Q 1230+0115, separated by 0.9° on the sky, provides an example of 8 absorbers and 7 galaxies aligned along a possible filamentary structure at least $20h_{70}^{-1}$ Mpc long. While some strong ($\mathcal{W} > 400$ mÅ) Lyα absorbers may be gas in the extended gaseous halos of individual galaxies, much of the local Lyα "forest" appears to be associated with the large-scale structures of galaxies and some with voids.

Subject headings: intergalactic medium — quasars: absorption lines — ultraviolet: galaxies — galaxies: halos

1. Introduction

Since the discovery of the high-redshift Lyα forest over 25 years ago, these abundant absorption features in the spectra of QSOs have been used as evolutionary probes of the intergalactic medium (IGM), galaxy halos, large-scale structure, and chemical evolution. In the past few years, these discrete Lyα lines have been interpreted theoretically by N-body hydrodynamical models (Cen et al. 1994; Hernquist et al. 1996; Zhang et al. 1997; Davé et al. 1999) as arising from baryon density fluctuations associated with gravitational instability during the epoch of structure formation.

Most previous studies of the low-z IGM (Bahcall et al. 1993; Jannuzi et al. 1998; Weymann et al. 1998) have been performed with the Faint Object Spectrograph (FOS) aboard the Hubble Space Telescope (HST). These studies, in general, characterized the Lyα absorbers with rest-frame equivalent widths ($\mathcal{W}$) greater than 0.24 Å. These studies detected some features with $\mathcal{W} \leq 240$ mÅ, but, because of sensitivity function considerations, performed most of their Lyα statistics for $\mathcal{W} \geq 240$ mÅ. A great deal more information can be gained from studying the more numerous weak Lyα lines, using the moderate-resolution first-order gratings (19 km s^{-1}) on the HST spectrographs, either the G160M grating on the Goddard High Resolution Spectrograph (GHRS) or the Space Telescope Imaging Spectrograph (STIS) with medium resolution first-order gratings. With these instruments, the Colorado group has engaged in a long-term program to study the very low redshift ($z < 0.069$) Lyα forest. In Paper I (Penton, Stocke, & Shull 2000a) we described our GHRS/G160M observations and presented a catalog of Lyα absorbers toward 15 extragalactic targets. We detected 81 "definite" Lyα absorbers at a significance level $\geq 4\sigma$ and 30 additional "possible" absorbers at $3 - 4\sigma$ in the redshift range $0.002 < z < 0.069$ over a total pathlength $c\Delta z =$ 116,000 km s^{-1} ($\Delta z = 0.387$). In Paper II (Penton, Shull, & Stocke 2000b) we described the physical properties of these Lyα absorbers and compared them to their high-redshift counterparts.

An important result from Paper II is that the number density of absorbers per unit redshift rises sharply at Lyα rest-frame equivalent widths $\mathcal{W} \leq 100$ mÅ ($N_{\rm HI} \leq 10^{13.4}$ cm^{-2} for Doppler parameter $b = 25$ km s^{-1}; see Figure 8 in Paper II). This corresponds to a region in column density probed only by observations made with the GHRS or STIS and medium resolution first-order or echelle gratings. Both the column density distribution and

---

[1]Based on observations with the NASA/ESA Hubble Space Telescope, obtained at the Space Telescope Science Institute, which is operated by the Association of Universities for Research in Astronomy, Inc. under NASA contract No. NAS5-26555.

[2]Also at JILA, University of Colorado and National Institute of Standards and Technology.

its evolution with redshift suggest that these lowest column density clouds are a population physically distinct from those at higher column density, as has been widely discussed for the high-z Lyα forest for some time (**?**, e.g.,)]Sargent87. The two-point correlation function (TPCF) of local Lyα absorbers has no excess power over a random distribution except for $\Delta v \leq 200$ km s^{-1}, where a modest excess of close pairs is observed (Figure 21 in Paper II, and Impey, Petry & Flint 1999; hereafter IPF99). As we show in § 6, the Lyα TPCF has a much lower amplitude than the galaxy-galaxy TPCF at z=0.

Several previous investigations used the detection of relatively nearby Lyα absorbers to determine whether a physical relationship exists between Lyα absorbers and galaxies. Using HST Key Project data (Bahcall et al. 1993; Jannuzi et al. 1998), **?**)L95 hereafter]Lanzetta95 proposed that most, if not all, low-z Lyα absorbers arise in extended halos of galaxies. This claim, limited to those absorbers detected in FOS data ($\mathcal{W} \geq 0.24$ Å), was based upon an observed inverse correlation between $\mathcal{W}$ and the impact parameter from the QSO sightline to the nearest galaxy. An extension of the L95 work by **?**)C98 hereafter]Chen98 strengthened the observed inverse correlation but found little evidence that this correlation depended on any other galaxy property, aside from galaxy luminosity. This is contrary to what would be expected if the size of the gaseous galaxy halo were due to internal properties or structures in the galaxies (e.g., star formation rate and thus galaxy color, Hubble type, etc.). In the most recent work by this group (Chen et al. 2001), the authors conclude that all galaxies, regardless of Hubble type or recent star formation history, possess extensive gaseous halos of near unity covering factor; e.g., an L^* galaxy has a halo extent of $260h_{70}^{-1}$ kpc. We assume a Hubble constant of H_0=70 h_{70} km s^{-1} Mpc^{-1} throughout the paper. The limitations of the L95 and C98 work are that their sample was based on only the strongest absorbers at low z, and that they did not consider absorbers for which no nearby galaxy was detected. Based upon a detection of a nearby galaxy in only about 1/3 of the cases, L95 and C98 extrapolate their result to all nearby Lyα absorbers, assuming that absorbers for which no nearby galaxy was detected are associated with galaxies too faint to be discovered using their survey.

Tripp, Lu, & Savage (1998a) and Stocke et al. (1995) claim that neither of the C98 extrapolations are justified and that the absence of correlations with other galaxy properties argues against the "galaxy halo" model. Numerical simulations (Davé et al. 1999) are able to reproduce the L95 inverse correlation without extended galaxy halos, because it arises from the presence of both galaxies and Lyα absorbers within the same large-scale filaments. Therefore the connection suggested by L95 may be only coincidental, not physical or causal. The simulations also suggest that weaker absorption lines will be found farther from galaxies and will fail to show the inverse correlation seen for the stronger absorbers, as has been observed (Stocke et al. 1995; Tripp, Lu, & Savage 1998a; IPF99).

By using Lyα lines detected with the GHRS, Morris et al. (1993), Stocke et al. (1995), Tripp, Lu, & Savage (1998a), Grogin & Geller (1998), and IPF99 investigated the relationship between weak Lyα absorbers and galaxies. The better far-UV sensitivity of the GHRS allowed these studies to detect absorbers at substantially lower redshifts and thus much nearer than typical Key Project detections (i.e., at $z \leq 0.2$ compared to $0.1 \leq z \leq 1.6$). The superior GHRS resolution allowed the detection of much weaker absorbers ($\mathcal{W} \geq 0.1$ Å for the low-resolution grating studies of Tripp, Lu, & Savage (1998a) and IFP99 and $\mathcal{W} \geq 0.015$ Å for the medium-resolution studies of Morris et al. (1993) and this work) albeit over shorter pathlengths than the Key Project data.

None of these studies found any compelling evidence for a close association between galaxies and absorbing clouds. On the contrary, the initial study of Morris et al. (1993) along the sightline to 3C 273, found nearest bright-galaxy neighbors at $\geq 200\ h_{70}^{-1}$ kpc, with some nearest galaxies more than $1 h_{70}^{-1}$ Mpc away from some clouds. Followup scrutiny of the nearest of these clouds, in the southern extremities of the Virgo Cluster at cz=1000–1600 km s^{-1}, failed to find any galaxies within 100-150 h_{70}^{-1} kpc of these absorbers down to impressively low limits ($M_B \geq -13$; Rauch, Weymann & Morris 1996). These include low surface brightness galaxies, as would be detected optically at central surface brightness limits of ≥ 26.4 mag arcsec^{-2} (Rauch, Weymann, & Morris 1996) or by 21 cm emission (**?**, $M_{HI} \geq 10^7\ h_{70}^{-2}\ M_\odot$;)]VG93. Substantiating these results, Stocke et al. (1995) and Shull et al. (1996) found some nearby, low-z, Lyα absorbers in "voids" in the bright CfA galaxy redshift survey regions, with nearest bright galaxies several Mpc distant. Because both the brighter and the fainter galaxies "avoid the voids", these authors concluded that at least some local Lyα absorbers were not associated with galaxies at all. A nearest-neighbor galaxy analysis using the bright survey data suggested that, while these low column density absorbers do not cluster with galaxies as strongly as galaxies cluster with other galaxies, neither are they randomly distributed. They are slightly closer to galaxies than would be expected by chance. This result confirmed the earlier statistical results of Morris et al. (1993), using the 3C 273 sightline (**?**, see)for an analysis of this result in terms of several populations of clouds, some closely associated with galaxies, some not at all associated]Mo94. Stocke et al. (1995) suggested that these results are compatible with $\sim 2/3$ of these absorbers being associated with large-scale structures ("filaments") in the galaxy distribution with the remaining absorbers distributed entirely randomly. The much lower amplitude in the TPCF of these low-$N_{\rm HI}$ absorbers, compared to the galaxy TPCF, is consistent with the filament interpretation (IPF99, Paper II).

More recently, **?**)GG98 hereafter]Grogin98 used a small number (18) of Lyα absorbers found in the region of the CfA galaxy redshift survey to determine that Lyα absorbers are found at locations random with respect to galaxy density. Their smoothing kernel of 2–

5 h_{70}^{-1} Mpc allowed them to reconstruct a robust measure of Galactocentric galaxy density, compared to using the nearest-neighbor galaxy distance, which is prone to biases due to the magnitude limits of the galaxy survey employed. However, these smoothing lengths may be too large to assess accurately the possible physical association between absorbers and large-scale structure suggested by earlier work. IPF99 addressed this difficulty by determining both nearest-neighbor distances and smoothed galaxy densities for 11 Lyα absorbers in the Virgo supercluster region using a galaxy survey complete to $M_B \leq -16$. This impressive work finds that, while there is some bias in using nearest-neighbor distances to L^* galaxies, the distances to fainter galaxies ($L \geq 0.04L^*$) are still too large (240-1320 h_{70}^{-1} kpc for all but one absorber) to be considered as galaxy halos. Further, when smoothed using 2 h_{70}^{-1} Mpc spheres, Lyα absorbers are found in intermediate, not random, regions of galaxy density, supporting earlier speculations to this effect by Mo & Morris (1994) and Stocke et al. (1995). While IFP99 is the most comprehensive study of the relationship between Lyα absorbers and galaxies to date, it is still limited by the small number of absorbers studied (11) and the location of these absorbers within the Virgo supercluster region alone.

In this paper (Paper III), we use the 81 Lyα absorbers, whose discovery was reported in Paper I and analyzed in Paper II, in conjunction with currently available galaxy redshift survey data to explore the relationship between the low-z Lyα absorbers and bright galaxies. These sightlines are scattered across the sky, with only two targets behind the Virgo supercluster (3C 273 and Q 1230+0115). Our analysis uses the nearest-neighbor galaxy distribution of our absorber sample and also looks for correlations between the Lyα absorbers and large-scale galaxy structures (supercluster filaments and voids) that these galaxy surveys reveal. In § 2, we describe our Lyα sample and the galaxy catalog, which is based on the February 8, 2000 version of the Center for Astrophysics (CfA) redshift survey, plus a few other "pencil-beam" optical and H I surveys along specific sightlines using multi-object optical spectroscopy or 21 cm imaging spectroscopy from the Westerbork Synthesis Radio Telescope (WSRT) and the Very Large Array (VLA).

To examine the relationship of the Lyα absorbers to the 3-D galaxy distribution along each sightline, we use the "pie diagrams" in right ascension and declination and the tables of nearest galaxy neighbors presented in Paper I. We also develop a galaxy-absorber sample that is consistent in galaxy coverage, to avoid biases due to galaxy survey incompleteness. Our restricted sample (called the $4\sigma L^*$ sample) is composed of 46 Lyα absorbers of $\geq 4\sigma$ significance, located in regions of the local Universe where the galaxy catalogs are complete down to L^* galaxies, or below. In § 3, we use this sample to examine galaxy–absorber "coincidences" and the distribution of nearest-neighbor galaxies. We combine our galaxy detections and non-detections with the results of several other surveys in an attempt to determine whether most Lyα absorptions can be explained as arising from extended galaxy

halos. We also compare the nearest-neighbor distribution of our $4\sigma L^*$ sample to the galaxy-galaxy nearest-neighbor distribution, and to a random-galaxy distribution within the same galaxy survey regions. In § 4 we explore the relationship between Lyα absorbers and galaxy filamentary structures, both in terms of an individual example, the close pair of sightlines towards 3C 273 and Q 1230+0115, and by using statistical methods on the GHRS $4\sigma L^*$ sample. In § 5 we explore the properties of Lyα absorbers in galaxy superclusters and voids in terms of the Lyα absorber frequency, $d\mathcal{N}/dz$, as a function of $\mathcal{W}$. In § 6 we compare the two-point correlation function of galaxy halos to that derived in Paper II for Lyα absorbers. Finally, § 7 summarizes the most important conclusions drawn from these various comparisons and outlines work in progress that will improve the current results (e.g., in Penton, Stocke & Shull, 2002, we will incorporate an additional 15 sightlines observed with HST/STIS).

2. Sample of Absorbers and Galaxies

2.1. CfA Galaxy Pie Charts

In Paper I, we presented heliocentric "pie diagrams" in right ascension and declination versus heliocentric radial velocity for all 15 HST targets in our GHRS survey. These pie diagrams indicate the spatial positions of the CfA Redshift Catalog galaxies relative to our target sightlines and the detected Lyα absorbers, assuming a pure Hubble flow. The February 8, 2000 version of this catalog (Huchra et al. 1992) contains ∼120,000 galaxies with velocities less than 100,000 km s^{-1}, including several large sky areas where complete, magnitude-limited surveys have been completed (see § 2.3).

All Lyα absorber velocities were reported in Paper I in the LSR velocity scale, established by aligning the velocity centroids of the Galactic S II $\lambda\lambda$1250, 1253, 1259 absorption lines with the dominant Galactic 21-cm emission. We selected this velocity scale instead of the HST/GHRS wavelength solution owing to the possibility of an improper wavelength scale caused by poor target centering in the large science aperture (LSA). To convert our LSR Lyα absorber velocities to heliocentric velocities, we assumed that the solar velocity with respect to LSR is +20.0 km s^{-1} towards (α=18:03:50.3;δ=+30:00:17; epoch J2000). Due to this process, we estimate conservatively that the typical velocity accuracy of the Lyα absorbers is ±10 km s^{-1}. Our accuracy is limited by the centroid uncertainty of the Gaussian fit, added in quadrature with the coincidence accuracy of the dominant H I 21-cm emission and the S II absorption lines. The error in the mean of the Gaussian fit is listed individually for each line detected in Table 2 of Paper I. The accuracy of the CfA redshift catalog galaxy recession velocities is variable (median velocity error of 34 km s^{-1}; mean velocity error of 43 km s^{-1}). Herein, the absorbers of Paper I are converted to heliocentric velocities to match the galaxy data.

2.2. Nearest-Neighbor Galaxies

In the upper panel of Figure 1, we display a histogram of the nearest-neighbor distances from each of our 81 4σ absorbers to the nearest CfA redshift survey galaxy. The distribution is split at the median $\mathcal{W}$ (56 mÅ, or $\sim 10^{13.1}$ cm^{-2} for $b = 25$ km s^{-1}). The dark bins are the histogram for the weaker absorbers, while the grey bins are the stronger absorbers. A two-sided Kolmogorov-Smirnov (K-S) test indicates that the weaker and stronger distributions are different at the 99.9% (4σ) confidence level. We suspect that the weaker and stronger absorbers may sample different populations with different space distributions.

In Paper I we listed the nearest 3 galaxies for all SL>3σ Lyα absorbers in our sample, with information on galaxy morphology, location, dimensions, velocity, and magnitude taken from the Revised CfA Redshift Catalog unless otherwise indicated. The line of sight (LOS) distance from the absorber to the galaxy uses a "retarded Hubble flow" model (Morris et al. 1993; Stocke et al. 1995) which accounts for peculiar galaxy motion and galaxy rotation by decreasing the reported total absorber-galaxy distance compared to a "pure Hubble flow" model where LOS distance is given by $c(z_{abs} - z_{gal})H_0^{-1}$. In the "retarded Hubble flow" model, we consider any galaxy within ± 300 km s^{-1} of the recession velocity of an absorber to be at the same distance from us as the absorber, and we decrease all LOS distances by $c(z_{abs} - z_{gal})H_0^{-1}$, if $c(z_{abs} - z_{gal}) < 300$ km s^{-1}, or by 300 km s^{-1} if $c(z_{abs} - z_{gal}) > 300$ km s^{-1}. All three-dimensional distances quoted herein use this "retarded Hubble flow" model for computing distances long the line-of-sight and assume Euclidean geometry, given the small redshifts involved. Therefore, our 3D nearest-neighbor distances should be considered conservative lower limits.

While the ±300 km s^{-1} tolerance on matching absorber to galaxy velocities is a somewhat arbitrary choice, we note several reasons that brought us to this selection. First, halo stars (L95) and high velocity gas associated with our own galaxy extend to these velocities. Secondly, the rotation curves of the most massive galaxies extend to these velocities. While this value is somewhat greater than typical velocity dispersions of galaxy groups and supercluster "filaments", it is typical of the full range of velocities therein (**?**, e.g.,)]Ramella92. Finally, while L95 allowed a ±250 km s^{-1} leeway for "association" between absorbers and galaxies, both the FOS absorber velocities and the faint galaxy velocities obtained by L95 are less accurate than those used here. So, to be conservative in the sense of being more inclusive of possible absorber-galaxy "associations" (and thus more open to the L95 hypothesis that all absorbers are extended galaxy halos), we use this somewhat larger range for absorber-galaxy velocity differences. In a "pure Hubble flow" model (i.e., no velocity tolerance), the 3D distances between galaxy and absorber would be even larger.

2.3. The $4\sigma L^*$ Sample

Because the CfA redshift survey is a flux-limited survey and does not contain uniform galaxy information as a function of position on the sky, some of our sightlines are better suited than others for nearest-neighbor analysis. Four of our 15 sightlines (I ZW 1, MRK 335, MRK 421, and MRK 501) pass through well-surveyed regions of the February 8, 2000 CfA survey. In an earlier publication (Stocke et al. 1995) we used these sightlines to investigate probable galaxy-cloud relationships. To date, the well-surveyed regions of the CfA catalog

that are complete to $m_B \leq 15.5$ are (in 1950 coordinates):

$$8^h \leq \alpha \leq 17^h \; ; \; 2.^\circ 5 \leq \delta \leq 44.^\circ 5 \qquad \text{First 6 CfA Slices}$$

$$20^h \leq \alpha \leq 4^h \; ; \; -2.^\circ 5 \leq \delta \leq 90^\circ \qquad \text{Southern Galactic Cap}$$

$$4^h \leq \alpha \leq 8^h \text{ and } 17^h \leq \alpha \leq 20^h \; ; \; 0^\circ \leq \delta \leq 45^\circ \qquad \text{[LGL]}.$$

Galaxies in the low Galactic latitude survey (LGL) are taken from Marzke, Huchra, & Geller (1996), while the Southern Galactic Cap data are taken from Huchra, Vogeley, & Geller (1999). The CfA catalog also includes all galaxies in the Morphological Catalog of Galaxies (MCG, Huchra et al. 1993), complete to $m_B \leq 15.0$ in the following region:

$$20^h < \alpha < 5^h \; ; \; -17.^\circ 5 \leq \delta \leq -2.^\circ 5 \qquad \text{[MCG]}.$$

One sightline (MRK 509) lies in this region of the sky. The CfA catalog also includes all galaxies in the merged Zwicky-Nilson catalog (Nilson 1973), complete to $m_B \leq 14.5$ in the regions:

$$b \geq 40^\circ \; ; \; \delta \geq 0^\circ \text{ and } b \leq 30^\circ \; ; \; \delta \geq -2.^\circ 5 \qquad \text{[NZ40]}.$$

This region is known as the North Zwicky 40 (NZ40), and it includes the sightlines of MRK 279, MRK 290, and MRK 817. In addition, Grogin, Geller, & Huchra (1998) (GGH) have extended the CfA survey down to m_B=15.7 in the region:

$$11.5^h \leq \alpha \leq 13.5^h \; ; \; -3.^\circ 5 \leq \delta \leq 8.^\circ 5 \qquad \text{[GGH]},$$

which includes the sightlines towards 3C 273 and Q 1230+0115. Finally, the second southern sky redshift survey (SSRS2; da Costa 1999) contains the PKS 2155-304 sightline and is complete down to $m_B \leq 15.5$ in the region:

$$(-40^\circ \leq \delta \leq 2.^\circ 5 \; ; \; b \leq -40^\circ) \text{ or } (\delta \leq 0^\circ \; ; \; b \geq 35^\circ) \qquad \text{[SSRS2]}.$$

The CfA catalog also includes the Bright Galaxy Redshift Catalogue (BGRC), which is an all-sky catalog complete to m_B=13.21.

In addition, five of our objects (3C 273, H 1821+643, MRK 335, MRK 501, and PKS 2155-304) have undergone optical multi-object spectroscopy and/or "pencil-beam" H I surveys with WSRT or VLA. The 3C 273 sightline was observed by Morris et al. (1993) with the Fiber Spectrograph on the Las Campanas 2.5m du Pont Telescope using the 2D-FRUTTI detector. Redshifts were obtained over region of radius $> 1^\circ$ centered on 3C 273. The H 1821+643 sightline was observed by Tripp, Lu, & Savage (1998a) using the WIYN+HYDRA in a 1° circular field of view. These optical surveys are reported to be complete down to $m_B \leq 19$ over a full 1° field and 72% complete to $m_B \sim 18$ over a

20' radius, respectively. However, as with any fiber survey, some galaxies might be missed due to fiber positional misalignments and positioning constraints. The MRK 335 and PKS 2155-304 sightlines were observed with the VLA (van Gorkom et al. 1996; Shull et al. 1998). The PKS 2155-304 sightline was observed over the velocity ranges 3562–6637 km s^{-1} and 16,230–17,530 km s^{-1} to an H I mass limit well below that of an L^* spiral galaxy. MRK 335 was observed with the VLA over the velocity range 1635–2635 km s^{-1} at a resolution of 25 km s^{-1}. The MRK 501 sightline was observed over the velocity ranges 4385–5385 km s^{-1} and 7240–8240 km s^{-1} with a resolution of 17 km s^{-1} (van Gorkom et al. 1996). Table 1 summarizes the galaxy information available for each sightline, including by column: (1) sightline target name; (2) the Zwicky (blue) magnitude limit of the catalog along this sightline; (3) the catalog names as described above; and (4) the velocity limit (cz_c) at which the catalog magnitude limit equals L^*. Velocities along the sightline less than the velocity limit (cz_c) are complete to magnitudes fainter than L^*.

Owing to our concerns over Lyα absorbers with significance levels $3\sigma \leq SL < 4\sigma$, we only include absorbers with $SL \geq 4\sigma$ in our analysis. To achieve some consistency in our nearest-neighbor sample, we adopt the following condition for inclusion in our $4\sigma L^*$ sample: the absorber must reside at a velocity and location on the sky in which the CfA redshift catalog (or other survey) is inclusive of all galaxies down to at least L^*. In the Zwicky (blue) magnitude system, an L^* galaxy has an absolute magnitude of $M_B^* = 5 \log h_{70} - 19.57$ (Marzke et al. 1994); for the objects in the well-surveyed CfA regions, which are complete for $m_B \leq 15.5$, this velocity cutoff is $cz \leq 7230$ km s^{-1}. Table 1 summarizes the velocity restrictions for each of our sightlines. Note that the PKS 2155-304 sightline is unusual, since its velocity coverage is not contiguous. Under these velocity and significance level restrictions, there are 46 absorbers in our $4\sigma L^*$ sample. Table 2 presents all 4σ absorbers, sorted by velocity with the following information by column: (1) target name (an asterisk indicates pre-COSTAR data), (2) the absorber heliocentric radial velocity and its error in km s^{-1}, (3) the rest-frame equivalent width ($\mathcal{W}$) and its error in mÅ, (4) whether this absorber is included in the $4\sigma L^*$ sample, (5) the CfA redshift catalog name of the nearest galaxy to this absorber, (8) the total Euclidean absorber-galaxy distance (D_{tot}, assuming the "retarded Hubble flow" model; see § 2.3), (6) the apparent Zwicky blue magnitude of this galaxy, and (7) the heliocentric radial velocity of this galaxy. When calculating absorber-nearest galaxy distances, we do not restrict ourselves to L^* or brighter galaxies, but consider all known galaxies in the field. Notice that, owing to the peculiar velocity allowance ($\pm$300 km s^{-1}) assumed here, several absorbers are paired with the same nearest known galaxy.

Table 1. Completeness Limits for our $4\sigma L^*$ Sample.

Target	m_b[a]	Catalog[b]	cz_c Limit[c] (km s^{-1})
3C273	19.00	GGH & Morris et al. (1993)[d]	$cz_c < 36233$
AKN120	13.21	BGRC	$cz_c < 2519$
ESO141-G55	13.21	BGRC	$cz_c < 2519$
FAIRALL9	13.21	BGRC	$cz_c < 2519$
H1821+643	18.00	Tripp, Lu, & Savage (1998a)[e]	$cz_c < 22784$
IZW1	15.50	South Gal Cap	$cz_c < 7230$
MARK279	14.50	N Zwicky 40	$cz_c < 4562$
MARK290	14.50	N Zwicky 40	$cz_c < 4562$
MARK335	15.50	South Gal Cap	$cz_c < 7230$
MARK335	···	VLA - van Gorkom et al. (1996)	$1635 < cz_c < 2635$
MARK421	15.50	2nd CfA Slice	$cz_c < 7230$
MARK501	15.50	1st CfA Slice	$cz_c < 7230$
MARK501	···	WSRT; van Gorkom et al. (1996)	$cz_c < 8240$
MARK509	15.00	MCG	$cz_c < 5743$
MARK817	14.50	N Zwicky 40	$cz_c < 4562$
PKS2155-304	15.50	SSRS2	$cz_c < 7230$
PKS2155-304	···	VLA HI	$16230 < cz_c < 17571$
Q1230+0115	15.70	GGH	$cz_c < 7927$

[a]Blue (Zwicky) magnitude limit of the indicated catalog along this sightline.

[b]Galaxy catalog used in determining nearest neighbors. The Bright Galaxy Redshift Catalog (BGRC), Southern Galactic Cap, North Zwicky 40, GGH, SSRS2, MCG, and CfA slices are taken from the February 8, 2000 version of the CfA redshift catalog; see text for acronym definitions.

[c]Velocity cutoff limit for which the indicated catalogs are complete down to L^* galaxies, assuming H_0= 70 km s^{-1} Mpc^{-1}.

[d]CfA + 1°-radius 2D-FRUTTI galaxy survey complete to $m_B \sim 19$.

[e]CfA + 20'-radius WIYN/HYDRA galaxy survey 72.4% complete at $m_B < 18$.

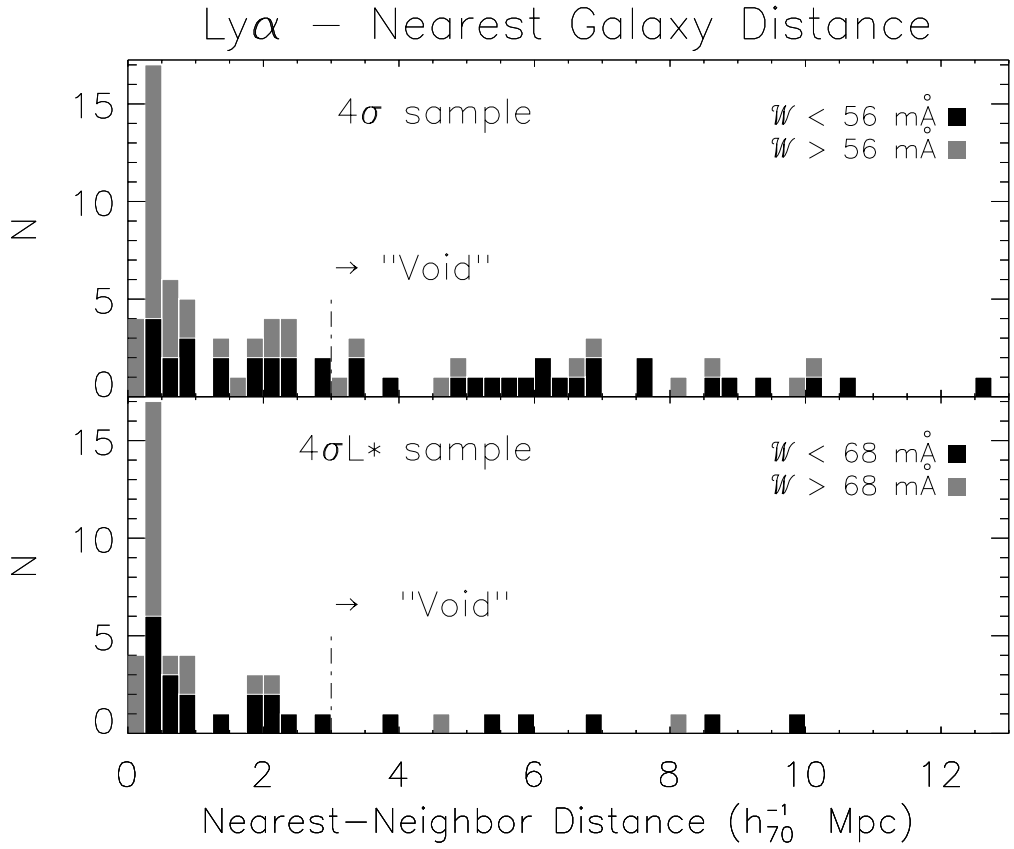

Fig. 1.— The upper panel displays a histogram of the nearest-neighbor distance to a CfA catalog galaxy for our 81 $SL \geq 4\sigma$ Lyα absorbers, split at the median $\mathcal{W}$ (56 mÅ). Each $250h_{70}^{-1}$ kpc bin should be considered an upper limit on 3D nearest-neighbor distance (D_{tot}), since the location of all galaxies is not known. Because our sightlines pass through regions of varying completeness in the CfA catalog, this distribution is non-uniform and possibly skewed towards larger nearest-neighbor distances. The lower histogram is for our restricted $4\sigma L^*$ Lyα sample (46 absorbers, see § 2.3), split at its median $\mathcal{W}$ (68 mÅ). In both median split samples, a K-S test indicates that the two subsamples are drawn from different parent populations at $> 99.3\%$ significance level. We identify the 8 absorbers in the lower ($4\sigma L^*$) panel with nearest-neighbor distances >3 h_{70}^{-1} Mpc as "void absorbers".

Table 2. Definite ($SL \geq 4\sigma$) Lyα features, listed in order of increasing velocity.

Target	cz_{abs} (km s^{-1})	$\mathcal{W}$ [a] (mÅ)	In[b] $4\sigma L^*$ sample ?	Nearest Galaxy	D$_{tot}$[c] (Mpc)	m$_B$[d]	cz_{gal} (km s^{-1})
∗3C273	1013 ± 6	369 ± 36	Y	12285+0157	0.17	15.60	1105
Q1230+0115	1487 ± 6	138 ± 42	Y	A1225+0152	0.27	16.30	1298
∗3C273	1583 ± 6	373 ± 30	Y	A1225+0152	0.18	16.31	1298
Q1230+0115	1664 ± 9	385 ± 94	Y	12308+0147	0.28	18.55	1643
Q1230+0115	1743 ± 7	241 ± 99	Y	12308+0147	0.28	18.08	1643
Q1230+0115	1857 ± 13	142 ± 81	Y	12308+0147	0.28	17.31	1643
MARK817	1919 ± 9	29 ± 13	Y	14332+5934	0.28	18.45	1920
∗MARK335	1961 ± 6	229 ± 30	Y	00025+1956	0.10	18.45	1950
MARK817	2083 ± 5	135 ± 15	Y	14332+5934	0.28	18.45	1920
∗3C273	2287 ± 7	35 ± 30	Y	A1225+0258	0.40	17.10	2329
∗MARK335	2291 ± 12	81 ± 26	Y	N7817	0.45	18.88	2310
Q1230+0115	2298 ± 6	439 ± 57	Y	A1228+0116	0.16	18.88	2289
MARK509	2549 ± 6	209 ± 32	Y	A2028-1821	4.66	17.99	2314
∗PKS2155-304	2630 ± 15	42 ± 40	Y	A2156-3128	0.70	...	2786
∗PKS2155-304	2782 ± 16	36 ± 22	Y	A2156-3128	0.70	15.60	2786
MARK421	3035 ± 6	86 ± 15	Y	A1102+4120	2.14	...	2988
∗PKS2155-304	4028 ± 12	21 ± 11	Y	N7201	2.77	...	4452
AKN120	4057 ± 8	48 ± 18	N	A0510-0036	0.87	...	4284
∗MARK335	4265 ± 14	33 ± 16	Y	00008+2150	2.25	16.10	4455
MARK290	4652 ± 7	60 ± 18	N	A1542+5722	1.65	...	4287
∗MARK501	4659 ± 10	161 ± 43	Y	16510+3927	0.52	14.42	4625
MARK817	4668 ± 10	23 ± 11	N	14293+5528	6.54	...	5291
∗PKS2155-304	4949 ± 7	64 ± 23	Y	A2157-3025	0.33	16.30	5187
∗PKS2155-304	5010 ± 7	82 ± 22	Y	A2157-3025	0.33	16.30	5187
MARK817	5074 ± 6	207 ± 14	N	14293+5528	4.78	16.30	5291
∗PKS2155-304	5116 ± 7	218 ± 20	Y	A2157-3025	0.33	16.30	5187
MARK817	5222 ± 7	25 ± 7	N	14293+5528	4.78	17.40	5291
MARK279	5234 ± 7	30 ± 10	N	A1310+6745	8.89	17.40	5994
∗PKS2155-304	5615 ± 7	29 ± 15	Y	A2157-3025	1.86	15.70	5187
∗PKS2155-304	5670 ± 8	39 ± 16	Y	A2200-2909	2.32	20.60	5658
MARK817	5779 ± 7	34 ± 13	N	14293+5528	5.56	15.70	5291
∗MARK501	5990 ± 7	55 ± 46	Y	16310+3727	8.50	16.00	5309
MARK817	6241 ± 6	37 ± 8	N	A1414+6042	5.12	15.50	6595
FAIRALL9	6255 ± 9	22 ± 9	N	A0105-5820	3.32	15.50	5914
∗MARK335	6266 ± 6	130 ± 14	Y	00036+1928	0.82	16.34	5936
MARK279	6360 ± 7	58 ± 7	N	14010+6943	1.28	13.90	6293
MARK279	6433 ± 6	40 ± 7	N	14010+6943	1.28	13.90	6293
AKN120	6750 ± 7	53 ± 13	N	05071-0018	2.84	16.00	6961
MARK279	6913 ± 5	65 ± 8	N	A1401+7005	3.04	...	6430
MARK290	7071 ± 8	23 ± 10	N	A1505+6310	10.73	...	6584
FAIRALL9	7112 ± 8	32 ± 10	N	A0106-5837	6.76	16.00	7796
MARK817	7316 ± 13	17 ± 7	N	I1049	6.91	12.70	6728
H1821+643	7325 ± 5	298 ± 20	Y	Tripp1	0.87	16.00	7207
MARK290	7349 ± 6	21 ± 7	N	A1505+6310	12.51	17.00	6584

Table 2—Continued

Target	cz_{abs} (km s^{-1})	$\mathcal{W}$ [a] (mÅ)	In[b] $4\sigma L^*$ sample ?	Nearest Galaxy	D_{tot}[c] (Mpc)	m_B[d]	cz_{gal} (km s^{-1})
∗MARK501	7521 ± 17	53 ± 36	Y	17048+4107E	5.31	17.50	7852
H1821+643	7537 ± 9	50 ± 24	Y	Tripp1	0.97	15.00	7207
MARK279	7767 ± 6	48 ± 9	N	N5607	6.00	15.20	7595
MARK817	7785 ± 11	28 ± 9	N	14212+6010	7.57	15.60	8520
MARK279	7845 ± 10	21 ± 10	N	N5607	6.00	14.90	7595
H1821+643	7853 ± 7	40 ± 17	Y	18197+6340E	1.34	...	7756
∗3C273	7870 ± 11	33 ± 18	Y	A1228+0205	0.94	15.50	7593
AKN120	7884 ± 21	20 ± 25	N	A0509-0045	2.32	15.50	7888
H1821+643	7941 ± 8	68 ± 38	Y	Tripp2	0.34	15.60	8250
AKN120	7977 ± 5	147 ± 22	N	A0509-0045	2.32	15.60	7888
AKN120	8037 ± 7	65 ± 17	N	A0509-0045	2.32	15.60	7888
∗MARK501	8748 ± 7	66 ± 57	N	16572+4012	2.22	15.60	8714
∗3C273	8830 ± 8	114 ± 25	Y	A1226+0211	0.40	16.00	8807
Q1230+0115	9239 ± 8	301 ± 49	N	A1227+0144	0.52	14.80	9281
FAIRALL9	9498 ± 6	84 ± 13	N	A0114-6153	8.61	15.30	8818
∗3C273	9830 ± 17	46 ± 22	Y	A1225+0223	0.39	16.70	9752
FAIRALL9	11650 ± 7	16 ± 8	N	A0101-5726	9.44	16.70	11114
FAIRALL9	11930 ± 10	22 ± 9	N	A0120-5934	10.10	13.83	12927
FAIRALL9	12099 ± 18	30 ± 28	N	A0120-5934	7.73	14.39	12927
FAIRALL9	12202 ± 6	28 ± 7	N	A0120-5934	6.30	14.39	12927
H1821+643	12317 ± 6	64 ± 15	Y	18421+6358	6.94	14.39	12369
FAIRALL9	12416 ± 29	19 ± 23	N	A0120-5934	3.47	14.39	12927
PKS2155-304	13589 ± 6	101 ± 18	N	A2143-2933	10.15	...	14030
∗3C273	14689 ± 7	140 ± 25	Y	A1224+0230B	1.90	15.65	14860
∗3C273	14984 ± 14	46 ± 22	Y	A1224+0230B	1.90	16.15	14860
∗3C273	15239 ± 33	52 ± 40	Y	A1224+0230B	2.21	16.15	14860
∗3C273	15928 ± 19	64 ± 33	Y	A1223+0238	9.81	...	14986
PKS2155-304	16201 ± 5	346 ± 23	N	A2155-3033A	0.58	...	16200
PKS2155-304	16322 ± 15	62 ± 34	Y	A2155-3033A	0.58	...	16200
PKS2155-304	16922 ± 7	43 ± 37	Y	A2155-3033B	0.44	...	17093
PKS2155-304	16970 ± 9	389 ± 68	Y	A2155-3033B	0.44	16.58	17093
PKS2155-304	17116 ± 9	448 ± 79	Y	A2155-3033B	0.44	16.30	17093
PKS2155-304	17710 ± 6	139 ± 21	N	A2156-3017	3.39	15.30	17179
PKS2155-304	18071 ± 7	99 ± 20	N	A2156-2900	6.50	15.30	17739
∗3C273	18270 ± 24	47 ± 28	Y	A1229+0222	5.98	15.30	18889
∗3C273	19031 ± 12	47 ± 22	Y	A1229+0222	3.91	18.30	18889
∗3C273	19953 ± 6	297 ± 25	Y	A1222+0249	8.05	17.69	20661

Note. — A ∗ preceeding the sightline name indicates a pre-COSTAR HST observation.

[a]Rest-frame equivalent width.

[b]Y if the absorber is included in our $4\sigma L^*$ sample, N if not included.

[c]Euclidian absorber-galaxy distance assuming H_0=h_{70} 70 km s^{-1} Mpc^{-1}.

[d]Zwicky (blue) apparent magnitude of the nearest galaxy. For galaxies named Tripp#, the POSS II J-magnitude is given, which is roughly equivalent to m_B.

3. Galaxy - Absorber Relationships

3.1. Nearest-Neighbor Distributions

The lower panel of Figure 1 presents the nearest-neighbor galaxy distances for the 46 absorbers in the $4\sigma L^*$ sample. In this histogram, the stronger Lyα features, are displayed in grey bins, while the weaker features, W<68 mÅ, are displayed in dark bins. The choice of the 68 mÅ cutoff divides our restricted $4\sigma L^*$ sample equally by number and corresponds to $\log [N_{\rm HI}({\rm cm}^{-2})] = 13.15 - 13.18$ assuming a Doppler parameter of $b = 20 - 30$ km s^{-1} (see Papers I and II). A two-sided K-S test indicates that the stronger and weaker features are drawn from different populations at the 99.3% ($> 3\sigma$) confidence level, similar to the result obtained for the median split $SL \geq 4\sigma$ sample shown in the upper panel of Figure 1. This also confirms our earlier contention (Stocke et al. 1995) that the weak and strong Lyα features are distributed differently with respect to nearest neighbors, with the stronger features generally having closer nearest galaxy neighbors. Eighty percent of our stronger $4\sigma L^*$ absorbers have a nearest galaxy neighbor within $1h_{70}^{-1}$ Mpc, while only 45% of the weaker $4\sigma L^*$ absorbers have a known galaxy within $1h_{70}^{-1}$ Mpc.

Note that there is considerable spread in the nearest-neighbor distances in both the strong and weak absorber samples. If we define being in a "void" as lacking a nearest neighbor within 3 h_{70}^{-1} Mpc, then 8 (17%) of our $4\sigma L^*$ absorbers are in voids and 38 (83%) are not. Our definition of "void" is not entirely arbitrary, in that 3 h_{70}^{-1} Mpc is the median distance from a random point in the low-z Universe to the nearest galaxy (see § 3.2 below). In our full sample, 32 of 81 of our 4σ Lyα absorbers (40%) lie in voids according to the above definition, illustrating the need to restrict the sample region according to limiting magnitude. While our use of a "retarded Hubble flow" model could create an underestimation of the void fraction, we have used other "void" definitions guided by the Slezak et al. (1993) wavelet technique for identifying voids. This secondary methodology gives nearly identical results to the $3h_{70}^{-1}$ Mpc retarded Hubble flow definition. Interestingly, even if we exclude the 17 local supercluster absorbers, there are only 3 out of 17 absorbers in voids at $cz < 10,000$ km s^{-1} but 5 out of 12 at greater cz. The reason for this possible difference is not clear but maybe due either to the different galaxy survey methodology employed in these two redshift regimes (i.e., "pencil-beam" surveys at higher cz, CfA redshift survey at lower cz) or to the greater sensitivity of our GHRS spectra at higher cz, causing statistically weaker absorbers to be detected at higher cz.

Of these 8 "void" absorbers, only two are in the strong half of the sample ($\mathcal{W} > 68$ mÅ):

1. MRK 509 : nearest galaxy = 4.7 h_{70}^{-1} Mpc ; $\mathcal{W} = 209$ mÅ ; $cz = 2549$ km s^{-1}

(galaxy survey complete to $0.2L^*$ at this location)

2. 3C 273 : nearest galaxy = 8.0 h_{70}^{-1} Mpc ; $\mathcal{W} = 297$ mÅ ; $cz = 19,953$ km s^{-1}
(galaxy survey complete to $0.3L^*$ at this location)

Because of its proximity, the cz=2549 km s^{-1} absorber of MRK 509 is our best candidate for studying Lyα absorbers in low-z galaxy voids.

Even though the $4\sigma L^*$ sample in Table 2 is defined by having galaxy redshift survey data complete to at least L^*, there is still a possible distance-dependent bias in nearest-neighbor distances because lower z locations within the same survey region are more sensitive to lower luminosity galaxies. Absorbers at $cz_{abs} < cz_c$ limit in Table 1 have been surveyed to below L^* luminosities and so these absorber regions have fainter known galaxies. Thus, a distance dependent bias could be introduced into the $4\sigma L^*$ sample, as a result. Using their Virgo region sample, IPF99 showed that decreasing the luminosity limit of the galaxies surveyed does decrease the nearest-neighbor distance to some of their 11 absorbers, so that such an effect could be present in the $4\sigma L^*$ sample as well. The use of different types of surveys (i.e., wide-angle, shallow surveys, deep pencil-beam surveys and limited velocity range 21 cm surveys) might also create some bias. For example, the closest galaxy-absorber pair in the $4\sigma L^*$ sample is due to a galaxy at $D_\perp = 96 h_{70}^{-1}$ kpc from the $cz = 1950$ km s^{-1} absorber in the MRK 335 sightline, which was discovered in a pointed H I survey (van Gorkom et al. 1996). This galaxy at $M_R \sim -15$ ($0.04L^*$) and $M_{HI} = 4 \times 10^7 M_\odot$ is below the CfA redshift survey limit at that distance ($M_B = -16.7$) and so is the least luminous galaxy in any galaxy redshift catalog used herein.

In Figure 2 we show the nearest galaxy distances to absorbers in the $4\sigma L^*$ sample as a function of recession velocity. We discount the absorbers at $cz \leq 2000$ km s^{-1}, almost all of which have uncommonly close absorber-galaxy distances. These absorbers are nearly exclusively in the 3C 273 and Q 1230+0115 sightlines which penetrate the southern region of the Virgo cluster at $cz < 2000$ km s^{-1}. This figure shows that there is no evident correlation between absorber distance and recession velocity (correlation coefficient=0.45). Similarly, the mean distance to the nearest 3 galaxies is not strongly correlated with redshift (correlation coefficient=0.59). Are the small absorber-galaxy distances at $cz \leq 2000$ km s^{-1} a result of the lower luminosity limits for galaxies, or of a larger space density of galaxies in the Virgo region? The answer is not obvious based upon the present information, but to be safe we investigate the $4\sigma L^*$ sample, with and without the Virgo absorber-galaxy pairs. Despite the absence of a correlation in Figure 2, we devised comparison methods that substantially reduce, if not eliminate, the effect of any distance-dependent biases by using the same CfA redshift survey volume to measure the statistics of the comparison samples (see § 3.2).

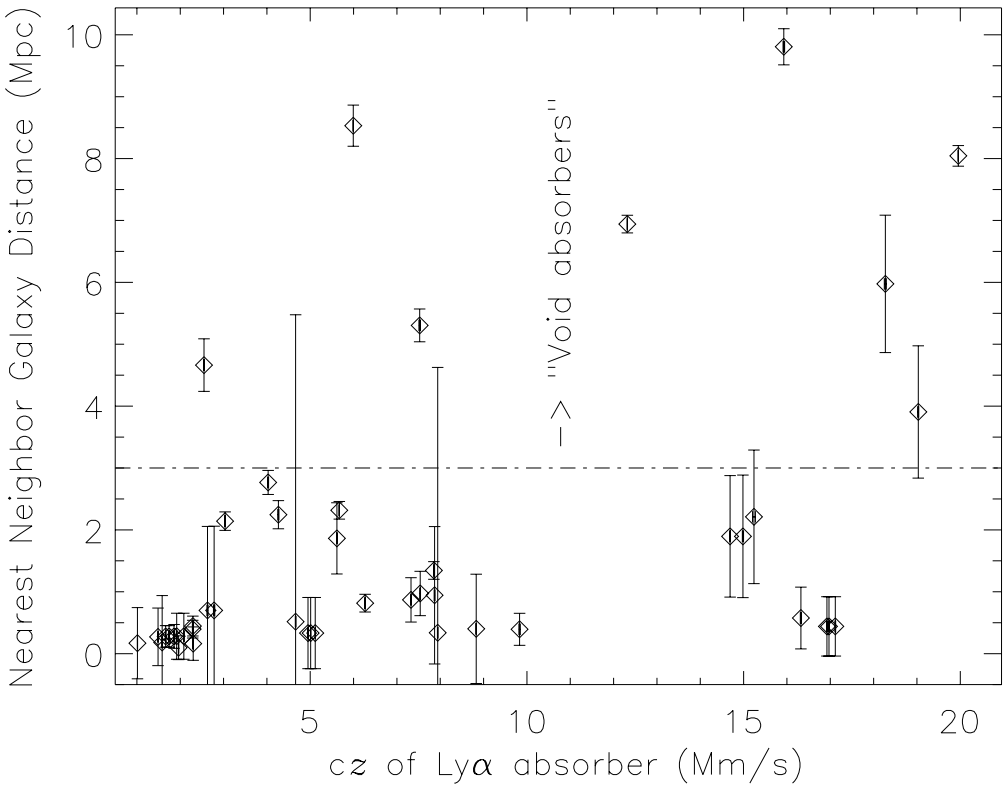

Fig. 2.— Nearest galaxy distances (D_{tot}) for all absorbers in the $4\sigma L^*$ sample, in h_{70}^{-1} Mpc. An absorber-galaxy "coincidence" is defined as any galaxy within 350 h_{70}^{-1} kpc of an absorber using our "retarded Hubble flow" model (see § 3.3). Eight "void absorbers" have $D_{tot} \geq 3$ Mpc.

3.2. Cumulative Distribution Functions

In order to achieve an unbiased comparison to our $4\sigma L^*$ sample of absorbers, we determine: (1) the galaxy-galaxy nearest-neighbor distribution and (2) the random location-nearest-neighbor galaxy distribution of the ∼5200 CfA galaxies in the first six CfA slices, that dominates our survey volume. Specifically, the distributions of nearest-galaxy-neighbor distances were calculated using the region covered by the first six CfA slices:

$$8.25^h < \alpha \leq 16.75^h \;\; ; \;\; 3.^\circ 5 < \delta < 43.^\circ 5 \;\; ; \;\; 575 < cz < 7230 \text{ km s}^{-1} \; .$$

The velocity constraints correspond to our lower spectral limit (1218 Å) and the L^* completeness limit. To avoid any possible "edge" effects, we consider only galaxies greater than ∼0.°5 from the edge of the "well-surveyed" regions defined in § 2.3. We have compared our absorbers to a random distribution based upon 250 sightlines through the above region that are consistent with the varying sensitivity, S(λ), and wavelength coverage of our spectra.

The random absorber location sample is simulated identically as in Paper II; for each pixel of each random spectrum (sightline), we compute the probability of a Lyα absorber occurring given our $d\mathcal{N}/d\mathcal{W}$ selection function. We combine this probability with the signal to noise (S/N) of each spectral location, to determine the probability, $P(\lambda)$, that a randomly placed absorber will occur at that location. If $P(\lambda)$ is greater than a uniformly distributed random number, then we locate an absorber at that pixel. As with the TPCF, because of our limited spectral resolution, two absorbers are not allowed to occur within 50 km s^{-1} of one another.

The galaxy-galaxy, random absorber-galaxy, and observed Lyα absorber-galaxy cumulative distribution functions (CDFs) are displayed for our $4\sigma L^*$ sample in Figure 3. The clustering of galaxies is revealed by the dashed line, which shows that $> 90\%$ of the galaxies in the $4\sigma L^*$ region are within 2 h_{70}^{-1} Mpc of another galaxy. For a random distribution (triple dot-dashed line) that matches the selection function of our $4\sigma L^*$ sightlines, only 27% are within 2 h_{70}^{-1} Mpc and 50% are within 3 h_{70}^{-1} Mpc of the nearest galaxy. The solid line shows our $4\sigma L^*$ absorber sample. The inclusion of the few absorbers at $cz \leq 2000$ km s^{-1}, that may be biased by being in the Virgo region (see Figure 2), does not alter the result significantly. It is clear that our $4\sigma L^*$ Lyα sample does not cluster with galaxies as strongly as galaxies cluster, but they are more clustered than a random distribution. K-S tests give only a 1×10^{-5} probability that our $4\sigma L^*$ absorber sample clusters with galaxies as strongly as galaxies cluster with other galaxies, and a 9×10^{-4} probability that the $4\sigma L^*$ absorber sample is randomly distributed with respect to galaxies. Figure 3 also shows that, while the median distance between L^* galaxies is $\sim 250 h_{70}^{-1}$ kpc, the median Lyα cloud-galaxy distance is $\sim 500 h_{70}^{-1}$ kpc. Because Lyα absorbers are typically twice as far away from bright galaxies as these bright galaxies are separated, it is problematic to associate these clouds with individual bright galaxy halos. The results shown in Figure 3 are similar to those in Morris et al. (1993), Stocke et al. (1995), Tripp, Lu, & Savage (1998a), and IPF99, although the different techniques used do not allow a more quantitative comparison with these earlier results. It has been suggested (Impey & Bothun 1997) that, because Lyα absorbers correlate with galaxies less strongly than galaxies correlate with galaxies, their clustering is similar to that of low-surface-brightness (LSB) galaxies. Impey & Bothun (1997) take one further logical step and associate Lyα clouds with LSB galaxies. This speculation remains an open question. We note that no LSB galaxies have been found close to any low column density Lyα clouds to our knowledge, including the pair of Virgo absorbers towards 3C 273, where sensitive limits have been set on their absence (Rauch, Weymann, & Morris 1996).

To further explore the possibility that the weaker and stronger Lyα absorbers sample different populations, we split the $4\sigma L^*$ sample into two distributions at $\mathcal{W}$ above and below 68 mÅ. The CDFs for these split samples are also shown in Figure 3. It is clear that the

stronger absorbers cluster more like galaxies, and the weaker absorbers appear to cluster more randomly, although neither sample is well-matched by the comparison samples. The K-S probability that the strong absorber-galaxy and the galaxy-galaxy distributions are drawn from the same parent distribution is 0.3% (4σ difference). The K-S probability that the weak absorber-galaxy and random-galaxy distributions are drawn from the same parent distribution is only 4×10^{-4}. Additionally, a K-S test indicates that the weak and strong Lyα samples differ at the 99.1% (3σ) confidence level. These results confirm our earlier suggestion (Stocke et al. 1995) of such a dichotomy, which was based on fewer absorbers.

The primary difference between the galaxy-galaxy and the strong absorber-galaxy nearest-neighbor distributions in Figure 3 is due to the two absorbers listed in §3.1. These two "void absorbers" are several h_{70}^{-1} Mpc away from the nearest known galaxy. In order to have these two distributions match each other statistically, very faint galaxies would have to be within $1 - 2h_{70}^{-1}$ Mpc of these absorbers. If these two "void absorber" are removed from the strong absorber sample, this sample still deviates from the galaxy-galaxy CDF at the 98.4% ($>3\sigma$) level. The very nearby "void absorbers" in the MRK 509 and MRK 421 sightlines are in regions already surveyed to $0.2L^*$ and $0.3L^*$ by the CfA survey data, respectively. Thus, the evidence is already strong that at least some higher column density absorbers are not physically associated with galaxies. New deeper galaxy surveys in the optical (McLin et al. 2002) and H I (Hibbard et al. 2002) extend this result to impressively low limits for these and other void absorbers. The absence of metal absorptions in the strong Lyα systems found in the PKS 2155-304 sightline at $cz \sim 17,000$ km s^{-1} (Shull et al. 1998) is further evidence that some higher column density Lyα absorbers are not "recycled gas" in extended galaxy halos.

?)GG98]Grogin98 recently used a subset of our $4\sigma L^*$ sample, in conjunction with the CfA redshift survey, to investigate the relationship between galaxies and Lyα clouds in a somewhat more robust manner. As shown by IPF99, the exact nearest-neighbor distance for each absorber depends upon the absolute magnitude limit. GG98 determined a galaxy density at each point within the CfA survey region by averaging over the 1–$3h_{70}^{-1}$ Mpc regions, using the detailed selection function of the survey to determine an averaged galaxy density at the location of each Lyα cloud. By doing this, GG98 avoided using just the nearest-neighbor galaxy distance as an indication of Lyα absorber environment. They also used the CfA survey mean luminosity function to correct for the presence of galaxies below the survey limit at each absorber. From this procedure, they found that Lyα clouds are located randomly with respect to the averaged galaxy density. We make the following comments about this work:

1. Although GG98 claim that their result is insensitive to their smoothing lengths, these

lengths are comparable to or larger than nearest-neighbor distances for 80% of our sample.

2. The GG98 sample contains roughly equal numbers of stronger and weaker Lyα absorbers by the definition of Figure 3.

3. Because the sample used by GG98 contains 5 absorbers that are no longer in our $4\sigma L^*$ sample (e.g., the cz=2060 km s^{-1} absorber in the 3C 273 sightline), this study should be revised with newer absorber data.

4. The GG98 analysis technique does not take into account the varying $\mathcal{W}$ sensitivity of the HST spectra, as we have done here.

In order to use the $4\sigma L^*$ sample to determine whether our current results are consistent with the GG98 analysis, we have repeated the nearest-neighbor analysis using the mean distance to the nearest 3 galaxies (see Table 10 of Paper I). We have generated galaxy-galaxy and random location-galaxy data to compare with the Lyα-galaxy data in a manner identical to the descriptions above. The use of the mean of the nearest three galaxy distances provides some smoothing of the galaxy environments, but on a scale more local to the Lyα absorbers than the GG98 analysis. Our results are shown in Figure 4, a CDF similar to Figure 3. To illustrate the importance of using the spectral sensitivity function, S(λ), when calculating the random CDF, we have also included the random CDF without using S(λ). As mentioned above, without considering S(λ), our Lyα CDF appears more random than it truly is. This suggests that, by not including the sensitivity of the Lyα survey, GG98 may have drawn the incorrect conclusion that Lyα absorbers are randomly distributed with respect to the galaxy density. New work is underway to utilize the GG98 technique on a much larger sample of absorbers, incorporating our S(λ) to revisit these results (Grogin et al. 2002).

3.3. Lyα Absorber Searches near Galaxies

Because of the suggestion by L95 that extended galaxy halos are the sources of Lyα absorption, we have searched for absorbers near known galaxies along our sightlines. For this purpose, we classify galaxy-sightline and galaxy-absorber matches into two categories: "coincidences" and "non-detections".

We define a "coincidence" as a $SL \geq 4\sigma$ absorber within 350 h_{70}^{-1} kpc of a galaxy using our "retarded Hubble flow" model. This distance was chosen to be inclusive of all "coincidences", based upon an earlier analysis of higher $\mathcal{W}$ absorbers by L95, but only five

of these are in as close proximity as the "associations" found by L95 (our impact parameter limit is 1.5 times the limits of galaxy halos suggested by L95; $230h_{70}^{-1}$ kpc). An absorber-galaxy coincidence does not necessarily imply that the absorber is gravitationally bound or physically connected with a galaxy in any way; for this present analysis it only implies proximity. In our full 4σ sample, we find that 14 of our 81 absorbers (17%) are "coincident" with 11 different galaxies. All of these "coincidences" involve absorbers in the $4\sigma L^*$ sample. Several galaxies are "coincident" with absorbers in both the 3C 273 and Q 1230+0115 sightlines up to $cz\sim$2300 km s^{-1}, although in most of these cases the velocity difference between the galaxy and the Lyα absorber in at least one of these sightlines is quite large (Table 3). Fully 2/3 of the "coincidences" are in the Virgo region of the 3C 273/Q 1230+0115 sightlines, suggesting that these matches are, in fact, truly coincidental; most occur in the region of highest galaxy density in our surveyed volume.

Table 3 lists, in order of increasing separation distance, galaxy-absorber information for the "coincidences". Eleven galaxies are listed for 21 "coincidences". For brevity, Table 3 lists a maximum of three associated galaxies for each absorber (complete information regarding these nearest galaxies can be found in Table 10 of Paper I). If only the nearest galaxy is listed, the number of "coincidences" drops to 16. Galaxy information is derived from the CfA survey, except where previously noted. Information in Table 3 includes by column: (1) sightline target name, (2) galaxy name, (3) the galaxy Zwicky magnitude, (4) the galaxy heliocentric radial velocity in km s^{-1}, (5) the galaxy-absorber 3D separation distance (D_{tot}) in h_{70}^{-1} kpc assuming our retarded Hubble flow model, (6) the heliocentric radial velocity in km s^{-1} for the associated Lyα absorber, (7) the rest-frame equivalent width ($\mathcal{W}$) of the Lyα absorber in mÅ, (8) the significance level (SL) of the Lyα absorber, and (9) whether the absorber is in our $4\sigma L^*$ sample. Because the D_{tot} values assume a retarded Hubble flow model, these 3D distances should be considered lower limits.

As previously mentioned, and indicated in Table 3, our closest galaxy-absorber pair is related to the 1963 km s^{-1} absorber in the MRK 335 sightline. The galaxy impact parameter at the velocity of the galaxy (1950 km s^{-1}) is $D_\perp = 96h_{70}^{-1}$ kpc. The "coincident" galaxy, detected by a 21 cm survey (van Gorkom et al. 1996), has an estimated $M_R = -15$ (0.04 L^*) and an H I mass $\sim 4 \times 10^7 M_\odot$.

Almost all of the "coincidences" are in the well-surveyed Virgo cluster region surrounding the 3C 273 and Q 1230+0115 sightlines. These include the Haynes & Giovanelli H I cloud (HG cloud hereafter; $cz_{gal} = 1105$ km s^{-1}), which is $116h_{70}^{-1}$ kpc off the Q 1230+0115 sightline but has no Lyα detection in the new Q 1230+0115 E140M spectrum to ≤ 20 mÅ (3σ). However, there is a Lyα detection in the 3C 273 spectrum at $cz_{abs} = 1013$ km s^{-1}, with an impact parameter (Table 4), and D_{tot} (Table 3) of $170h_{70}^{-1}$ kpc from the HG cloud.

Therefore, if the 3C 273 detection and the Q 1230+01115 non-detection are both probing the HG galaxy halo, that halo must be quite patchy or asymmetric. Bowen, Blades, & Pettini (1996) came to a similar conclusion involving the covering factors of galaxy "halos" using independent data. This is the only "non-detection" of a bright galaxy in our sample, by which we mean that no $> 3\sigma$ absorber is found within 350 h_{70}^{-1} kpc of a known galaxy assuming our retarded Hubble flow model.

In Figure 5, the solid '+'s present the Δv vs D_{tot} results given in Table 3 for all detected Lyα absorbers within $350h_{70}^{-1}$ kpc of a known galaxy. Also displayed, by the numerous dots, is the distribution expected for random galaxy-Lyα absorber coincidences using our retarded Hubble flow model. Due to our retarded Hubble flow 3D distance determination (D_{tot}), if the difference in velocity between the absorber and the nearest galaxy were > 300 km s^{-1}, the computed D_{tot} would become very large. The upper boundary of '+'s and dots in Figure 5 in due to this assumption. As implied by Figure 5, and confirmed by K-S tests, the observed distribution of "coincidences" shows no significant departure from random galaxy-absorber locations. K-S tests give an 88% probability that the Δv distribution of Lyα clouds with respect to the nearest galaxy is consistent with the random distribution. The D_{tot} results are also consistent with random coincidences. Therefore, our absorber-galaxy "coincidences" are statistically consistent with chance galaxy-absorber locations and are not indicative of any physical or causal relationship.

3.4. Equivalent Width versus Impact Parameter Relationship

Lanzetta et al. (1995), and more recently C98, used HST/FOS spectra of bright quasars observed by the Key Project Team (Bahcall et al. 1993) to study the association of nearest galaxies to Lyα clouds at $0.1<z<0.3$. C98 reported a distinct anticorrelation between absorber $\mathcal{W}$ and impact parameter to the LOS ($D_\perp$) out to 230 h_{70}^{-1} kpc, which led them to suggest that most galaxies are surrounded by extended gaseous halos of $\sim$230 h_{70}^{-1} kpc and that most or all Lyα absorptions arise from these extended galaxy halos. HST/FOS data have wavelength resolution of $\sim$1 Å and minimum detectable equivalent widths about 10 times greater than our HST/GHRS spectra. The FOS survey did contain some weaker absorbers, so there is some small overlap in $\mathcal{W}$ between the FOS and GHRS surveys. The minimum $\mathcal{W}$ used by L95/C98 is $\sim$400 mÅ, roughly 6 times higher than the median $\mathcal{W}$ studied herein. Because many or most of the L95/C98 Lyα absorptions correspond to metal-line systems and have substantially higher column density, the results in Figure 6 show that the L95/C98 conclusions may not be appropriate to extrapolate to weaker Lyα detections.

At high-z, it is still debated (Sargent 1987; Tytler 1987; Songaila & Cowie 1996,

Table 3. Galaxy-Lyα "Coincidences".

Target	Galaxy Name	m_B[a]	cz_{gal} (km s^{-1})	D$_{tot}$[b] (kpc)	cz_{abs} (km s^{-1})	$\mathcal{W}$ (mÅ)	SL	In $4\sigma L^*$ sample ?
MARK335	00025+1956	16.0	1950	96	1961	229	28.1	Y
Q1230+0115	A1228+0116	18.3	2289	162	2298	438	23.9	Y
3C273	12285+0157	15.6	1105	169	1012	369	34.8	Y
3C273	A1225+0152	16.3	1298	181	1012	369	34.8	Y
3C273	A1225+0152	16.3	1298	181	1583	372	42.0	Y
3C273	A1224+0146	NA	1275	231	1012	369	34.8	Y
3C273	12277+0254	15.3	1635	260	1583	372	42.0	Y
3C273	A1224+0146	NA	1275	261	1583	372	42.0	Y
Q1230+0115	A1225+0152	16.3	1298	271	1487	138	6.3	Y
Q1230+0115	12308+0147	15.3	1643	279	1487	138	6.3	Y
Q1230+0115	12308+0147	15.3	1643	279	1742	241	10.9	Y
Q1230+0115	12308+0147	15.3	1643	279	1663	384	16.9	Y
Q1230+0115	12308+0147	15.3	1643	279	1857	141	6.6	Y
MARK817	14332+5934	15.5	1920	281	2082	135	25.3	Y
MARK817	14332+5934	15.5	1920	281	1918	28	5.3	Y
Q1230+0115	12270+0107	17.0	2234	292	2298	438	23.9	Y
Q1230+0115	A1224+0146	NA	1275	293	1487	138	6.3	Y
PKS2155-304	A2157-3025	14.4	5187	332	4948	64	14.3	Y
PKS2155-304	A2157-3025	14.4	5187	332	5010	81	18.1	Y
PKS2155-304	A2157-3025	14.4	5187	332	5115	218	48.1	Y
H1821+643	Tripp2[c]	20.6	8250	337	7940	67	9.4	Y

Note. — An "concidence" is defined as any galaxy within $350h_{70}^{-1}$ kpc of one of our sightlines that coincides with a $SL \geq 4\sigma$ Lyα absorber assuming our "retarded Hubble flow" model. Some galaxies are associated with multiple Lyα absorbers, and some absorbers have multiple associated galaxies. We limit the number of "coincidences" per absorber to three.

[a]Blue (Zwicky) magnitude, where available.

[b]Total Euclidean distance (in h_{70}^{-1} Mpc) to the nearest absorber using our "retarded Hubble flow" model.

[c]The Tripp2 galaxy is taken from Tripp, Lu, & Savage (1998a).

Tytler et al. 1995, Weymann 1995) whether there are two distinct populations of H I clouds: metal-poor absorbers that do not cluster and higher column density ($N_{\rm HI}$ >10^{14} cm^{-2}) metal-bearing absorbers that cluster like galaxies. Tripp, Lu, & Savage (1998a) used GHRS/G140L+G160M spectra of H 1821+643 (G160M included in our sample) and a GHRS/G140L spectrum of PG 1116+215 with minimum $\mathcal{W}$ ∼50 mÅ to examine the $\mathcal{W}$ versus $D_\perp$ relationship. They concluded that the anticorrelation persists to 640 h_{70}^{-1} kpc, but at a significantly larger dispersion than for just the C98 data. In Figure 6, we collect $\mathcal{W}$ and $D_\perp$ from our study, C98, Morris et al. (1993), Tripp, Lu, & Savage (1998a), and IPF99. We also include our non-detections of § 3.3 and those of C98.

As indicated in Figure 3, it is rare to have a random sightline with an impact parameter from an $\sim L^*$ galaxy less than 1 h_{70}^{-1} Mpc. Therefore, since FOS and G140L spectra cannot detect absorbers with $\mathcal{W} <$ 50 mÅ, or $\log[\mathcal{W}(\text{Å})] < -1.3$, it not surprising that the lower left corner of Figure 6 is sparsely populated using galaxy surveys of fields that do not go exceptionally faint (as in the L95 and C98 studies). Galaxy detection surveys that extend significantly below L^* (van Gorkom et al. 1993, 1996; Shull et al. 1996; Rauch, Weymann & Morris 1997; IPF99) would be expected to find smaller impact parameters, by chance in some cases (see e.g., § 3.3 and IPF99 Figure 13). The upper right corner of Figure 6, with large impact parameters and high $\mathcal{W}$s, is also sparsely populated. Perhaps this is merely a consequence of the scarcity of large-$\mathcal{W}$ absorbers in galaxy voids. Our GHRS survey does not have sufficient pathlength to detect such rare, strong absorbers, but the FOS Key Project does, should such absorber systems exist. We do not know if any are present in the L95 and C98 samples, since, as pointed out by Tripp, Lu, & Savage (1998a), neither L95 nor C98 plot the absorbers for which they failed to discover nearby galaxies. We have not included the "failed searches" from C98 in Figure 6. However, the lower limits implied by their non-detections place 2/3 of their absorbers to the right of the dash-dot vertical ("void") line. We caution that the L95 & C98 galaxy searches do not go very deep and could have left nearby L^* galaxies undetected, to say nothing of dwarf or LSB galaxies.

In Figure 6 we overplot a linear fit that corresponds to the C98 data only and returns a high probability of correctly modeling their data alone (>99.99%). Even so, the C98 correlation is quite broad at any $\mathcal{W}$ or $D_\perp$, so that the high correlation coefficient may merely reflect the biases mentioned above against finding galaxy-absorber pairs in the upper left and lower right quadrants of Figure 6. When all the data in Figure 6 are fitted, the correlation coefficients indicate a low probability of correctly modeling the data (<0.01%). The solid line in Figure 6 is a linear fit to our GHRS data alone and also returns a low probability of correctly modeling our data (<8%).

As seen in Figure 6, the region with $D_\perp$> 200 h_{70}^{-1} kpc ($\log[D_\perp] > 2.3$) and $\mathcal{W} <$ 400 mÅ

($\log\left[\mathcal{W}\ (\text{Å})\right] < -0.4$) is a nearly uniform scatter plot. Based upon the low probability for the fits to the low-$\mathcal{W}$ absorbers in Figure 6, we conclude that the results of C98 and L95, the anticorrelation between galaxy impact parameter ($D_\perp$) and absorber $\mathcal{W}$, does not extend above $D_\perp$>200 h_{70}^{-1} kpc. In fact, when the non-detections of C98 are included (the triangles with downward arrows in Figure 6), it appears that the reported anticorrelation may not extend above $D_\perp$> 50 h_{70}^{-1} kpc ($\log\left[D_\perp(\text{kpc})\right] > 1.7$). This distance may be the full extent of gaseous halo material physically associated with the nearby galaxy. Alternately, gaseous halos may extend somewhat further, but with lower covering factor (**?**, see)]Mo00. In addition, it has been demonstrated (Davé et al. 1999; Linder 2000) that this anticorrelation can arise even if weaker absorbers are not associated with galaxies in any way.

Taken with the above discussion of the selection biases inherent in the L95 and C98 distributions of Figure 6, we conclude that, while some of the highest column density Lyα systems in the local Universe may be associated with the gaseous halos of nearby bright galaxies, the lower column density clouds show no evidence of extending this correlation. In fact, Davé et al. (1999) have reproduced the salient features of Figure 6, including the observed slope shown by the dotted line, using a N-body plus hydrodynamical simulation in which mass feedback from galaxies into the IGM is small. In other words, both the L95/C98 correlation at high $\mathcal{W}$ and the increasing scatter at low $\mathcal{W}$ in our data can be explained by these simulations. In Davé et al. (1999) this correlation is reproduced simply because galaxies and Lyα clouds both trace the same large-scale structure. The simulations also predict that the correlation should degrade towards lower column density because three distinct populations of clouds, with somewhat different relationships to galaxies, are involved: (1) cold, condensed clouds that are quite close to galaxies ($D_\perp \leq 30h_{70}^{-1}$ kpc) and are plausibly galaxy halos; (2) highly-ionized absorbers, shock-heated by infalling large-scale structure and thus near "filaments" of galaxies ($30h_{70}^{-1} \leq D_\perp \leq 300h_{70}^{-1}$ kpc); and (3) warm, diffuse photoionized clouds that are truly intergalactic and thus much more randomly placed relative to galaxies ($D_\perp \geq 300h_{70}^{-1}$ kpc). The L95 and C98 absorber samples appear to contain primarily type 1 and 2 clouds, while the GHRS studies consist of types 2 and 3. See IPF99 for a speculative division of local Lyα absorbers into these three types described by Davé et al. (1999).

The C98 results that the correlation in Figure 6 are largely independent of the properties of the nearby galaxy lends further support for the contention that this correlation is the result of large-scale structure alone, as Davé et al. (1999) predict. C98 found only a correlation with galaxy luminosity, but not with any star formation properties (e.g., Hubble type or color), which would certainly be expected if these absorbers were due to some pervasive feedback of gas from galaxies into the IGM. Additionally, the "failure" of the sensitive galaxy searches around low-z Lyα absorbers by Rauch, Weymann, & Morris (1996), van Gorkom et al.

(1993, 1996), Shull et al. (1996, 1998), and IPF99 plus the examples of local Lyα absorbers found in galaxy voids by Stocke et al. (1995) and this paper, adds considerable evidence to the contention that not all Lyα clouds arise in extended gaseous galaxy halos.

Finally, while some authors have suggested that many low column absorbers might be associated with low surface brightness (LSB) galaxies (Impey & Bothun 1997; Linder 2000), there are no current data supporting this suggestion. Specifically, Rauch, Weymann, & Morris (1996) searched the 3C 273 field for LSB galaxies at Virgo distances and found none; IPF99 found similar negative results in the Virgo cluster proper. Since many LSB galaxies are H I rich, they should be detected easily by H I images of Lyα absorber locations and have not been (van Gorkom et al. 1993, 1996; Shull et al. 1996; Hibbard et al. 2002). New H I and optical surveys are now in progress to address this suggestion further.

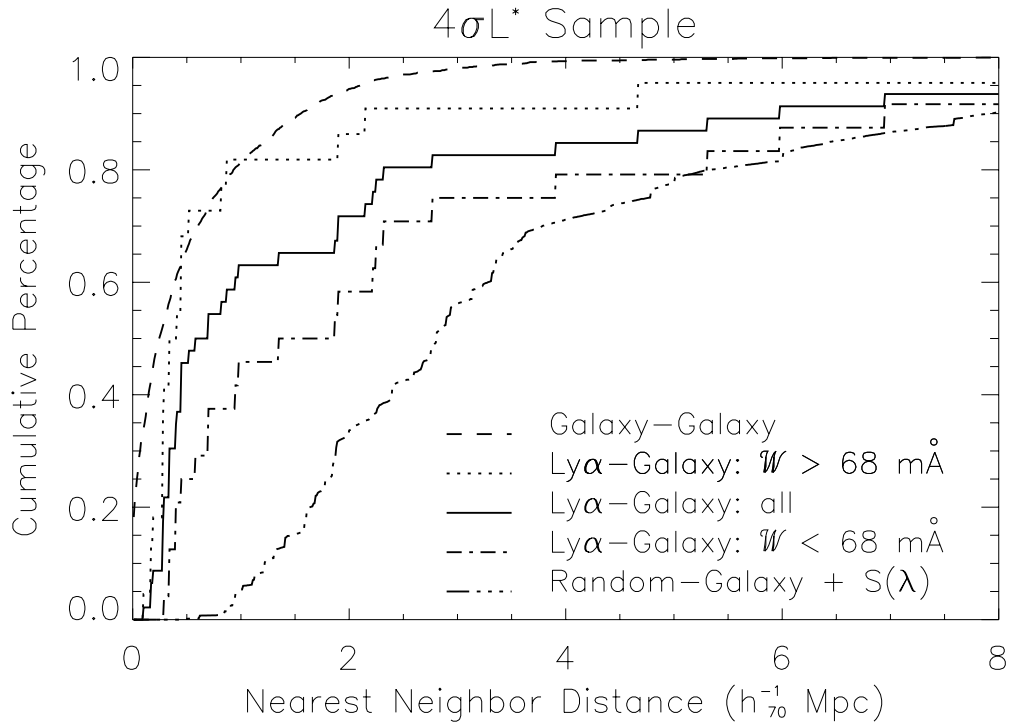

Fig. 3.— Nearest-neighbor cumulative distribution function (CDF) for our $4\sigma L^*$ sample (solid line, Lyα -galaxies). The dashed line indicates the CDF for the galaxy-galaxy nearest-neighbor distances in well-surveyed regions of the CfA redshift survey (see text). This curve shows the strong clustering of galaxies; 90% of the galaxies have nearest-neighbors within 2 h_{70}^{-1} Mpc. The triple dot-dashed line indicates the distribution expected for random locations within our survey volume accounting for our wavelength and sensitivity limits, S(λ), combined with our $d\mathcal{N}/d\mathcal{W}$ distribution. Dotted and dot-dashed lines show the CDF for our $4\sigma L^*$ sample when split above and below $\mathcal{W} = 68$ mÅ, the median of the $\mathcal{W}$-distribution. Fifty percent of randomly distributed locations are $\geq 3h_{70}^{-1}$ Mpc from the nearest CfA galaxy, suggesting a definition of a void as being locations $\geq 3h_{70}^{-1}$ Mpc from the nearest galaxy.

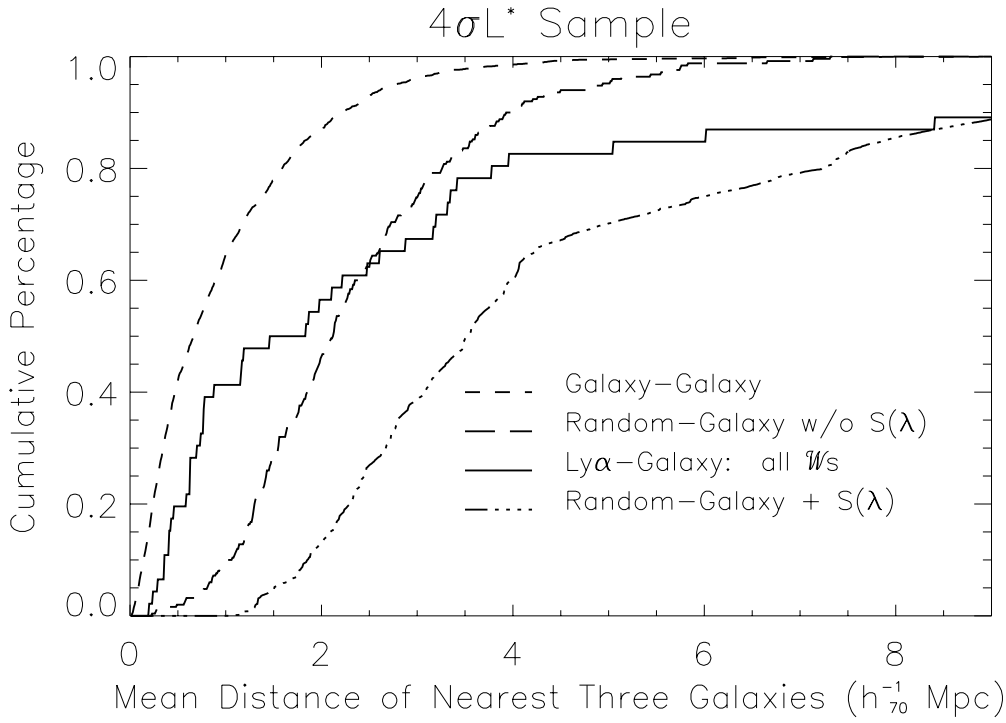

Fig. 4.— Nearest-neighbor cumulative distribution function (CDF) using the mean distance to the nearest three known galaxies. The short dashed line indicates the CDF for the galaxy-galaxy distances, the solid line gives the CDF for our $4\sigma L^*$ sample, and the dot-dashed and dashed lines show the CDF for random distribution with, and without, the inclusion of our sensitivity function, S(λ).

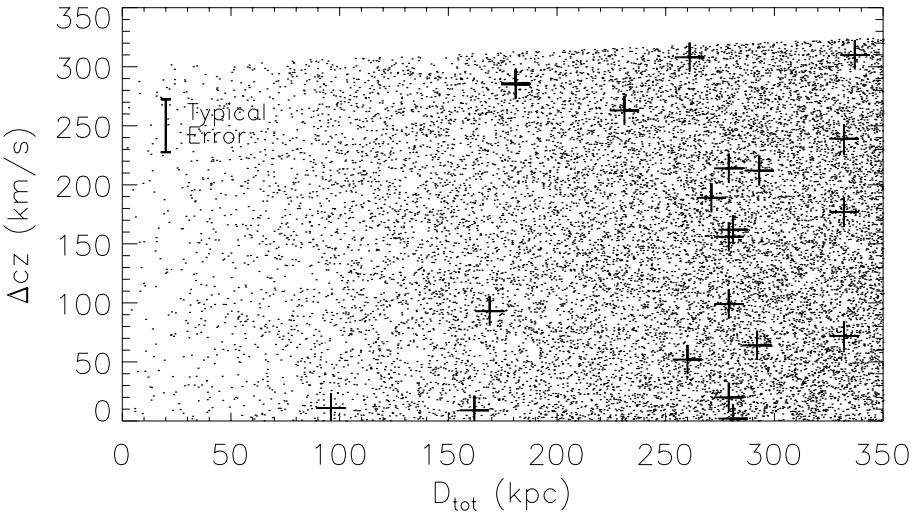

Fig. 5.— Galaxy-Lyα velocity difference (Δv) versus total, retarded Hubble flow, 3D distance (D_{tot}) between galaxy and absorber as presented in Table 3 (the '+'s). A random distribution of galaxies locations relative to the absorbers is shown by the numerous dots. Our observed distribution is consistent with a random distribution at the 88% confidence level.

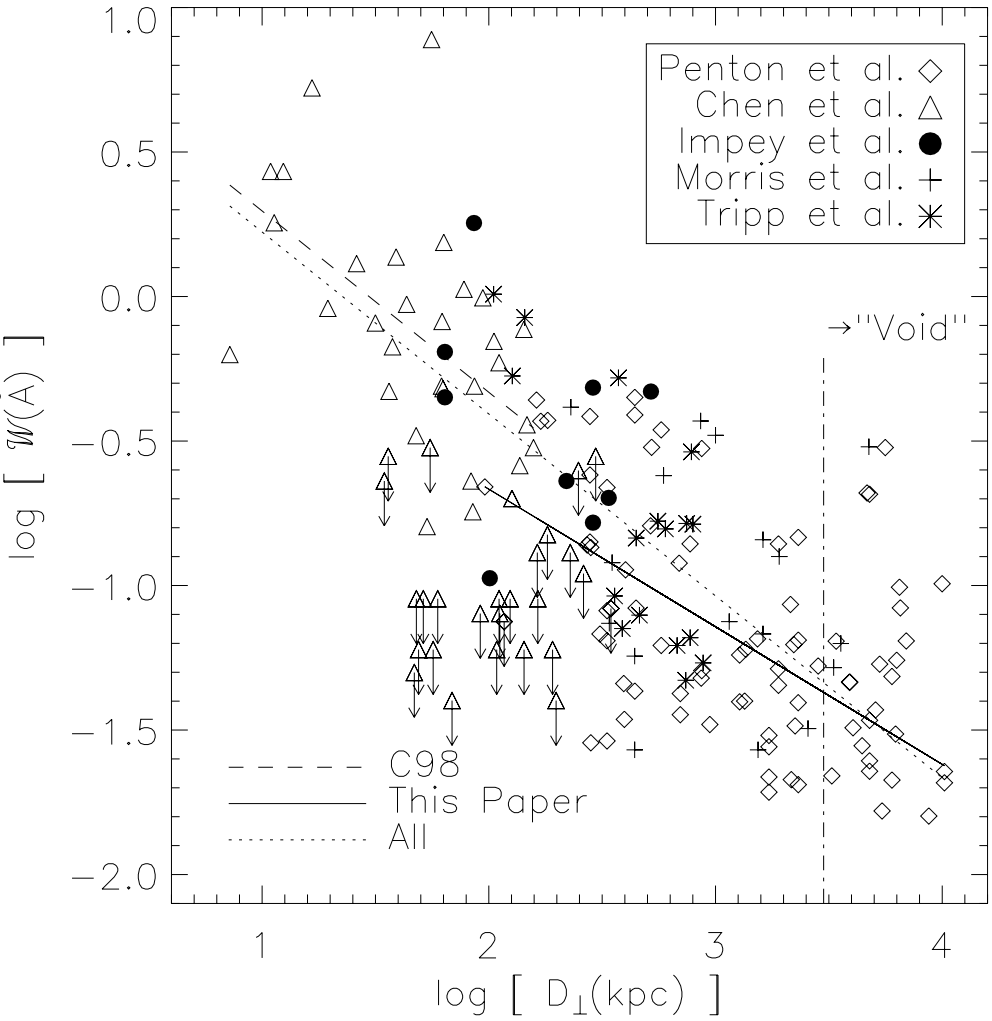

Fig. 6.— Lyα absorber equivalent width ($\mathcal{W}$) versus impact parameter ($D_\perp$) from the nearest galaxy to the line of sight. Since the absorber could be at a different velocity than the nearest galaxy, $D_\perp$ should be considered a lower limit to the actual galaxy-absorber distance. Non-detections are indicated by downward arrows, originating at the 3σ $\mathcal{W}$ upper limit. All distances are calculated assuming $H_0 = 70$ km s^{-1} Mpc^{-1}. The dashed vertical line indicates our "void" definition, $D_\perp > 3h_{70}^{-1}$ Mpc. The dashed linear fit corresponds to the C98 data only (triangles) and returns a high probability of correctly modeling those data (>99.99%). The dotted line, with a slope of -0.57, corresponds to a linear fit of all data and returns a low probability of correctly modeling all data (<0.01%). The solid line represents a linear fit to our $4\sigma L^*$ data alone and also returns a low probability of correctly modeling our data (<8%).

4. Lyα absorbers and Galaxy Filaments

4.1. The 3C 273/Q 1230+0115 field and absorbers

The proximity of the 3C 273 and Q 1230+0115 sightlines, 0.91° apart in the sky, provides an opportunity to look for common absorbers at very low z and thus to infer the sizes of Lyα clouds. Due to the depth of galaxy surveys in this region, these two adjacent sightlines also allow an important new method for relating Lyα absorbers to galaxies and large-scale structure. Over the range $1000 < cz < 2300$ km s^{-1}, these sightlines are separated by (230–550) h_{70}^{-1} kpc. Absorbers in that redshift range are located in the southern portion of the Virgo Cluster region. Updated column densities for the two strongest Virgo cluster absorbers along the 3C 273 sightline have been reported by Sembach et al. (2001) on the basis of FUSE spectra.

A digitized sky survey (DSS) image around 3C 273 and Q 1230+0115 is presented in Figure 7. Additionally, 1.1° "pie diagrams" for this sightline, centered halfway between the two targets, are shown in Figure 8. Unlike the pie diagrams in Paper I, each galaxy is given its own designating letter in Figure 8. Table 4 lists these galaxies and their relationship to the 3C 273 and Q 1230+0115 sightlines, including by column: (1) the galaxy name in the CfA redshift catalog, (2) the galaxy's heliocentric radial velocity in km s^{-1}; (3) and (4) the distance in h_{70}^{-1} kpc on the sky between the galaxy and the 3C 273 and Q 1230+0115 sightlines, respectively; (5) the letter designation for the galaxy as shown in Figure 8; (6) and (7) the heliocentric velocity of the closest Lyα absorber in the 3C 273 and Q 1230+0115 sightline respectively. Galaxies (a) and (b) are the closest to these sightlines and are shown in the image in Figure 7, as well. Galaxy (a), A1225+1052, is also known as the Haynes & Giovanelli H I cloud (Giovanelli et al. 1991) and is composed of two H I peaks, only one of which clearly contains starlight (Salzer 1991). Galaxy (b), 12285+0157, has been recently studied by Hoffman et al. (1998). Because of infall to the Virgo Cluster, velocity-dependent distance estimates of galaxies in this region are uncertain on the order of ∼1-2h_{70}^{-1} Mpc; we assume that these "streaming motions" affect galaxies and Lyα absorbers the same and do not introduce additional errors to the galaxy-absorber distances. In this Section we will continue to estimate distances using recession velocities and $H_0 = 70$ km s^{-1} Mpc^{-1}.

A 1° area around the 3C 273 sightline was surveyed for galaxies by Morris et al. (1993) complete to $m_B \sim 19$. This region lies within the southern extension of the CfA survey made by Grogin, Geller, & Huchra (1998). At $20h_{70}^{-1}$ Mpc or cz=1400 km s^{-1}, the Morris et al. (1993) magnitude limit implies that galaxies have been surveyed in this field down to $\sim 10^{-3}$ L^*. Further redshift survey work towards the 3C 273 and Q 1230+0115 sightlines is in progress (McLin et al. 2002).

Table 4. Galaxies in the 3C 273/Q1230+0115 Field

Galaxy Name	cz_{gal}[a] (km s^{-1})	$D_\perp$[b] to 3C 273	$D_\perp$[b] to Q1230+0115	Label[c]	cz_{abs}[d] 3C 273	cz_{abs}[e] Q1230+0115
A1225+0152	1298	182	271	a	1012	1487
12285+0157	1105	170	116	b	1012	1487
12308+0147	1643	483	279	c	1583	1663
12277+0254	1635	260	562	d	1583	1663
A1224+0146	1275	282	294	e	1012	1487
A1228+0116	2289	678	162	f	2287	2298
12270+0107	2234	677	293	g	2287	2298

[a]Galaxy recession velocity.

[b]Galaxy to line-of-sight (LOS) distance, perpendicular to the LOS (in h_{70}^{-1} kpc).

[c]Label corresponding to Figure 8.

[d]Velocity of nearest Lyα absorber along the 3C 273 sightline

[e]Velocity of nearest Lyα absorber along the Q 1230+0115 sightline

All eight definite absorbers (3 towards 3C 273 and 5 towards Q 1230+0115) and two possible Lyα absorbers (one in each sightline) are presented in the "pie diagram" of Figure 8 as large and small dashed circles respectively. Considering only the definite absorbers, there are two close velocity matches between the sightlines: the 1583 km s^{-1} (3C 273) absorber matches both with the 1489 and 1665 km s^{-1} (Q 1230+0115) absorbers. Additionally, a possible absorber at 2287 km s^{-1} (3C 273) is closely matched with a definite absorber at 2300 km s^{-1} (Q 1230+0115), which needs better 3C 273 data to confirm. At lower spectral resolution (e.g., FOS at 1 Å), the pair of close absorbers (1489 and 1665 km s^{-1}) in the Q 1230+0115 sightline would be blended and so would be paired with the 1583 km s^{-1} absorber in the 3C 273 sightline to form a single pair of "common absorbers". This pairing would suggest a transverse size for this Lyα cloud of $\sim 350 h_{70}^{-1}$ kpc, similar to values found at higher redshift (**?**, e.g.,)]Dinshaw95,Impey97. However, four definite absorbers have no counterpart in the other sightline, suggesting upper limits on Lyα absorber sizes comparable to, or smaller than, this value.

The information in Figure 7 can be interpreted in terms of the extended galaxy halo hypothesis of L95, in that both galaxies (a) and (b) are close enough to both sightlines to expect Lyα absorbers in both spectra by the hypothesis of L95. Indeed, one could plausibly assign both the 1489 km s^{-1} or 1665 km s^{-1} absorbers in Q 1230+0115 and the 1012 km s^{-1} or 1583 km s^{-1} absorbers in 3C 273 to A1225+0152 ($cz_{gal} = 1298 \pm 20$ km s^{-1}), giving that galaxy a $\sim 300 h_{70}^{-1}$ kpc gaseous halo down to approximate column densities of 10^{14} cm^{-2}. Although three of the four absorptions are at higher recession velocities than the systemic velocity of A1225+0152, the fact that this galaxy is actually two interacting systems is supporting evidence for this picture. The second H I emission peak is located $\sim 100 h_{70}^{-1}$ kpc to the SW of A1225+0152 (Giovanelli et al. 1991), and thus just off the right edge of Figure 7 with an elongated H I halo of diameter $215 h_{70}^{-1}$ kpc at $N_{\rm HI} = 2 \times 10^{18}$ cm^{-2}. It has been speculated that galaxy interactions can increase greatly the gaseous cross-sections of galaxies (Morris & van den Bergh 1994; van Gorkom et al. 1996), and this set of galaxies and absorbers offers a laboratory to test that hypothesis.

However, the other nearby galaxy, 12285+0157, offers a counter-example to this same hypothesis. While the 3C 273 spectrum has an absorber which plausibly could be associated with this galaxy, being only 100 km s^{-1} lower than the galaxy velocity, the spectrum of Q 1230+0115 has no absorption within several hundred km s^{-1} of the galaxy redshift. This is despite the fact that A12285+0157 is closer to the Q 1230+0115 sightline than to that of 3C 273 by a factor of 1.5. At the very least, these two sets of absorbers and galaxies suggest that very extended galaxy halos (if they exist) cannot be spherical with unity covering factor. This is contrary to the suggestion by L95 and C98 that galaxy halos are spherical with large covering factor (see § 4.2 and Bowen, Blades, & Pettini (1996) for further discussions).

Figure 8 suggests an alternative explanation, described by the dashed lines, in which galaxies and clouds in this region occupy a single large "filament" $> 20h_{70}^{-1}$ Mpc long, with an aspect ratio of >20:1. This possible alternative interpretation makes all but one of the observed definite absorbers "common" between these two sightlines. A further statistical test that Lyα absorbers lie in galaxy "filaments" will be presented in the next section. We await better S/N and resolution spectra for both of these targets, as well as more galaxy redshift survey data in this region to confirm this possible "filament". Figure 8 shows the value of performing sightline pair experiments at low z, where both galaxies and absorbers can be integrated into a common picture of large-scale structure.

4.2. Statistical Tests of Lyα Cloud Alignment with Galaxy Filaments

In this section we investigate the statistical relationship between local Lyα absorbers and large-scale structure using the distribution of CfA galaxies in (3-11) h_{70}^{-1} Mpc diameter spherical or cylindrical regions around each absorber. The purpose of this investigation is to determine whether the local Lyα absorbers preferentially align with the large-scale "filaments" of galaxies, to which the Lyα clouds are also plausibly related in numerical simulations (Davé et al. 1999). A possible example of such an alignment was presented in the last subsection.

Because the methodology used in this section is new and somewhat complicated, an overview is supplied in this and the next paragraph. The basic approach is similar to comparing the position angle of the absorber to galaxy impact parameter vector ("absorber PA") to the galaxy major axis, as in C98. Instead we use many nearby galaxies in a specified volume to compare the mean "absorber PA" to the major axis of the galaxy large-scale structure "filament", composed of these same galaxies. Much of the below discussion is devoted to describing how the "filament" major axis is determined using the mean PA of all galaxy-galaxy vectors. We do not presume that filamentary structure is present in each volume beforehand, just as measurement of a galaxy major axis does not presume a highly flattened structure. We simply use whatever galaxy distribution is present to find the "filament major axis" using the mean of all galaxy-galaxy vectors. As described in detail below, this procedure returns a distribution of PAs which, in the mean, has a full-width-half-maximum of $\pm 20°$. An important variable in this process is the size of the volume around each absorber, which determines the number of galaxies (N) to be included in this analysis. For our fiducial volume ($4.3h_{70}^{-1}$ Mpc scale size), a typical absorber has several tens of galaxies in this volume but "void absorbers" have only a few, while some very nearby absorbers in very well-surveyed galaxy regions have several hundred (we truncate $N \leq 200$

to avoid any few absorbers from dominating our statistics). Through experimentation we have found that volumes $\leq 3h_{70}^{-1}$ Mpc in scale size contain too few galaxies to determine an accurate "filament" PA; volumes $\geq 8h_{70}^{-1}$ Mpc in scale size are so big that they contain several "filaments" (this is evident in "pie diagrams" from the CfA redshift survey shown in Paper 1), also degrading the accuracy of the "filament" PA. For volumes between these two extremes the "filament" PA can be determined to a mean accuracy of ± 5 degrees (see discussion below).

Once the "filament" and "absorber" PAs are determined for each volume, we align all vectors to the "filament" PA and co-add the vectors from all volumes in the $4\sigma L^*$ absorber sample. We then cross-correlate the "filament" PAs with the "absorber" PAs. We then repeat this procedure using "absorber" PAs for a set of "fake" absorbers, randomly located in the same volumes, to supply a comparison baseline. The amount by which the cross-correlation function (CCF) for the real absorbers exceeds the CCF for the "fake", randomly-distributed, absorbers is the statistical significance to which absorbers are aligned with galaxy "filaments". Large statistical significances are found for most volumes, as described in detail in the paragraphs below.

To explore the possible relationship between the detected Lyα absorptions and galaxy filaments, we compared our $4\sigma L^*$ sample of absorbers to the large-scale galaxy distribution in the vicinity of each absorber. To do this, we extracted a constant-volume cylinder or sphere from the CfA survey centered on each absorber. The diameter of the sphere and the length and diameter of the cylinder were set to Δv=300 or 450 km s^{-1} (4.3 or $6.4h_{70}^{-1}$ Mpc). The choice of Δv=300 km s^{-1} matches our previous "retarded Hubble flow" model of $\pm$300 km s^{-1} and appears to be a good match to the scale of large-scale structure "filaments" (see below). Additional larger box sizes were also examined to correct for the uncertainties associated with inferring galaxy/absorber distances from redshifts without knowledge of their peculiar velocities (PVs). This is done by allowing an additional $\pm$150 km s^{-1} or $\pm$300 km s^{-1} in PV for both our spherical and cylindrical models. The rationale behind these modified models is to include filament galaxies with large peculiar velocities, which would, if interpreted as pure Hubble flow velocities, place them just outside the sample volume. But, this also includes many more galaxies with low PV at larger distances from the absorbers; i.e., with increasing PV allowance, the region of space and number of galaxies included in our sample increases. In addition, we explored the consequences of different extraction volumes by performing trials for smaller (Δv=200 km s^{-1}) and larger (Δv=600 and 800 km s^{-1}) sizes. We find that volumes smaller than 300 km s^{-1} are too small to include a large enough number of galaxies to define adequately the large-scale structure, while larger volumes ($\geq$ 600 km s^{-1}) include more than one large-scale structure "filament", making the large-scale structure more complicated to interpret (see the "pie diagrams" in Paper I).

For all CfA galaxies in the extracted volume, we first determine the best-fitting (α, δ, cz) plane ($cz = A + B\alpha + C\delta$) of the galaxies in the volume using a robust, χ^2 -minimizing fit. The algorithm reduces the impact of "outliers" which do not reside near the dominant plane, if any, of the galaxies in each extracted volume. Before determining the best-fit plane, we convert α, δ and cz to units of h_{70}^{-1} Mpc. Once the dominant plane has been identified, we rotate the galaxy coordinates (X,Y,Z) in Mpc so that the dominant plane is aligned perpendicular to the new Z$'$ axis for viewing. This alignment to the coordinate system (X$'$,Y$'$,Z$'$) attempts to remove any viewing angle effect and reduces our exploration to the simple question: When viewed from a consistent "face-on" viewing angle, do our detected absorbers show any preference to be aligned with the filamentary structure seen in galaxy clustering?

Once the extracted CfA regions have been rectified to consistent, face-on viewing angles, we calculate the two-dimensional (2D) position angles (PAs) for all galaxy-galaxy and absorber-galaxy pairs to produce the distribution of PAs for each volume. For all absorber volumes, the dominant galaxy-galaxy PA is located by fitting a Gaussian to the PA distribution and choosing the Gaussian center as the mean PA of the filament. The "raw" PAs are then adjusted to the Gaussian mean PA so that the adjusted distribution is centered at PA=0°; i.e., these adjusted, or aligned, PAs (APAs) are relative to the major axis of the dominant galaxy filament in each volume. Because all absorber volumes now have their PAs zero-pointed to the best-fit, local filament PA, we can co-add the galaxy-galaxy and absorber-galaxy APAs from all volumes into a single distribution. To prevent any one absorber volume from dominating the APA distribution, we use a randomly selected subsample of only 200 galaxies for any volume with more than 200 galaxies. The median number of galaxies in each region for each model are given in Table 5.

Figure 9 shows the "raw" PAs (RPA) for both the galaxy-galaxy and absorber-galaxy pairs in a spherical volume model with PV = $\pm$150 km s^{-1} and Δv= 450 km s^{-1} diameter. Figure 10 presents the APAs for the same model, and shows that regardless of absorber location, the galaxy-galaxy PAs have a very narrow peak ($\pm$20° FWHM). Thus, in the mean, the "filament" PA can be determined with an accuracy that is a fraction of this; i.e., $\pm$5° conservatively. The rather narrow peak for the galaxy-galaxy APA distribution in Figure 10 tells us that the filaments in our sample are not predominantly "sheetlike"; i.e. they do not fill the viewing plane when rectified to "face on". The broader distribution in the Lyα -galaxy APAs is simply due to the inherent number statistics (i.e., N versus N^2/2). Also shown in Figures 9 and 10 are "raw" PAs (RPAs) and APAs, respectively, for a comparison sample of random absorber locations within volumes of the same size and shape as the volumes from which the observed PA distributions were extracted. These random locations along our actual GHRS sightlines were constructed in an identical way as in Paper II and § 3.4,

accounting for the varying sensitivity and spectral coverage of our observations. Random APAs were also constructed for sightlines randomly placed throughout CfA survey regions of sky, using the median sensitivity function of our observations. This approach approximately matches our HST/GHRS observations in terms of number of sightlines passing through well-surveyed CfA regions (see § 2.3) from $575 \leq cz \leq 10,000$ km s^{-1}. The random APAs from these "all-sky" sightline simulations are nearly identical to our random individual sightline results.

To determine the significances of the differences between the galaxy-random absorber, galaxy-real absorber, and galaxy-galaxy APA distributions, we compare the cross-correlation functions (CCFs) of the APAs. For the galaxy-galaxy APAs, this is obviously the auto-correlation function. For each of our random methods, using our sightlines and the random ("all-sky") method, we performed N_{trial} Monte Carlo simulations, each one simulating our combined HST/GHRS observations, using the median sensitivity function, $S(\lambda)$, and our $d\mathcal{N}/d\mathcal{W}$ results from Paper II. The value of N_{trial} for each model is given in Table 5. For the "all-sky" trials, the median $S(\lambda)$ was applied.

In Figure 11 we present the CCFs for the Δv=300 and 450 km s^{-1}, PV=$\pm$0 and $\pm$150 km s^{-1} spherical models. Since these APAs have been adjusted to a zero point corresponding to the dominant PA of galaxy-galaxy vectors in each volume, the large peaks in these distributions indicate the same strong filamentary structure in the galaxy distribution along our sightlines as seen in Figure 10. To calculate the significance of our galaxy-absorber CCF over the random distribution, we compare the area in the central CCF peak to the random distribution. In Figure 11, the (small) error bars represent the 1σ standard deviations of the random "all-sky" CCFs. The extent of the central peak, over which we calculate the excess power in the absorber-galaxy CCF, is defined by the locations of zero CCF power in the galaxy-galaxy auto-correlation function (the filament width as defined by the galaxy locations). By dividing the difference in areas by the 1σ uncertainty inferred from the random trials, we determine the degree to which absorbers (and galaxies) align with filamentary large-scale structures. These absorber results are given in Table 5. Particularly, for the smaller volumes with no PV allowance, the excess power is large; $5 - 12\sigma$ for the various models. The PV = $\pm$300 km s^{-1}, Δv=450 km s^{-1} model creates a sample region that is the equivalent of 1500 km s^{-1}, or 21.4 h_{70}^{-1} Mpc along the line of sight. As seen from the pie diagrams in Paper I, this volume is much larger than most filamentary structures, hampering our ability to correctly identify the dominant filamentary plane and the dominant PA necessary for proper PA zero-pointing. Thus, we believe that the Δv=450 km s^{-1}, PV = $\pm$300 km s^{-1}, and larger volume models, sample too large a volume to determine accurately the local filamentary structure, causing our random and absorber results to appear similiar for both the spherical and cylindrical models. On the other hand, for the Δv<200 km s^{-1} volume with

no PV, there is little power in the random absorber CCF distribution; i.e., this volume is too small to allow the PA of the large-scale filamentary structure in the CfA catalog to be determined accurately. Thus, we believe that the first three models of each type (cylindrical, or spherical volume) in Table 5 give the most accurate representation of absorber-galaxy filament alignment.

These results agree with results from a simpler two-dimensional analysis which only considers position angle on the sky, without compensation for recession velocity. As seen from the significance levels in Table 5, these trials provide evidence that Lyα absorbers align with galaxy filamentary structures in the local Universe. Together with the lack of any correlation between low column density local Lyα absorbers and individual galaxies, this result is further proof that the Lyα absorbers are related to large-scale structure, not to individual galaxies, in agreement with numerical simulations. This result should also be contrasted with the C98 result that there is no statistical relationship between the "absorber PA" and the major axis of the nearest, bright galaxy. C98 interpret their result as meaning that galaxy halos are spherical with near unity covering factor. But, using a different technique, Bowen, Blades, & Pettini (1996) find a much lower covering factor of 0.4. Therefore, in the light of the present results, where an alignment between Lyα absorbers and galaxy filamentary structure has been found, the random location of Lyα absorbers with respect to the nearest galaxy may not be indicative of a galaxy halo property at all.

Table 5. Cross-Correlation Results for our $SL \geq 4\sigma$ Sample

Δv	PV[a]	Random	Spherical Model			Cylindrical Model		
(km s^{-1})	(km s^{-1})	Method[b]	SL[c]	N_{trials}[d]	median(N_{gal})	SL	N_{trials}	median(N_{gal})
300	0	A	12.6	41	74	14.8	44	74
300	150	A	11.1	16	76	6.8	15	76
450	0	A	12.0	19	72	8.3	27	70
450	150	A	< 1.0	29	74	< 1.0	33	73
300	0	G	8.4	41	68	11.8	44	68
300	150	G	10.2	16	69	6.0	15	69
450	0	G	9.1	19	68	8.3	27	69
450	150	G	< 1.0	29	70	< 1.0	33	71

[a]Peculiar velocity allowance.

[b]Method used to generate the random absorber sightlines; G (GHRS) uses our GHRS sightlines; A ("all-sky") uses a random distribution of sightlines through well-sampled regions of the CfA catalog.

[c]Significance Level above random as defined in the text.

[d]N_{trials} is the number of random trials used. Each random trial matches the number and pathlength of our GHRS sightlines.

[e]N_{gal} is the number of galaxies per detected absorber.

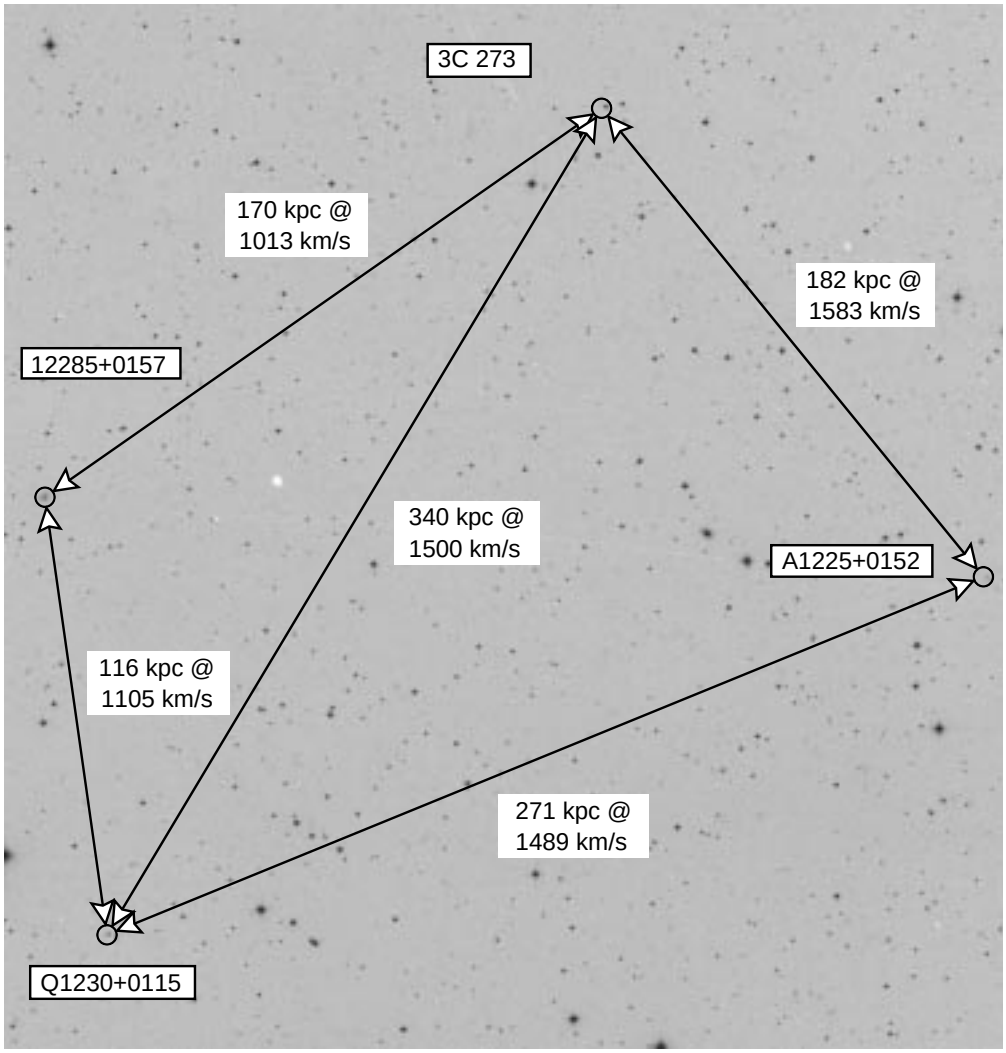

Fig. 7.— Digitized Sky Survey image of the 3C 273/Q 1230+0115 field. The image is $0.9^\circ \times 1.0^\circ$. Perpendicular distances ($D_\perp$) between the sightlines and from the A1225+0152 and 12285+0157 galaxies to the sightlines are indicated for H_0=70 h_{70} km s^{-1} Mpc^{-1}.

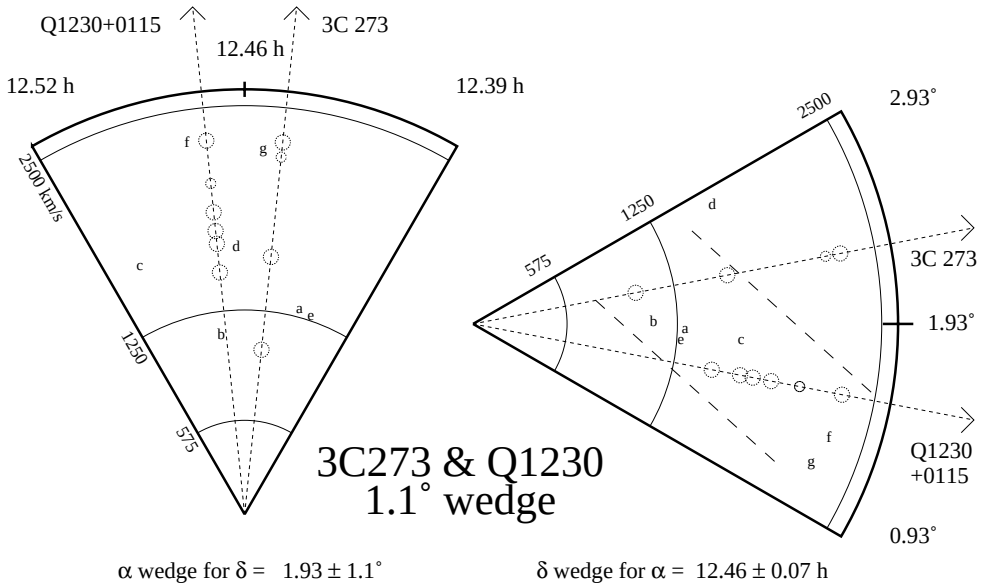

Fig. 8.— 1.1° pie diagram showing the 3C 273 and Q 1230+0115 sightlines, nearest galaxies, and absorbers with $V_{\rm hel}$ <2600 km s^{-1}. The Lyα absorbers are located with dashed circles; the larger circles are 4σ detections, the smaller circles are 3σ detections. The arc at 575 km s^{-1} indicates the lower velocity limit of our Lyα detections, corresponding to our spectral limit of $\lambda \geq 1218$ Å. The long-dashes in the declination (right) pie diagram outline the possible filamentary structure associated with both galaxies and absorbers.

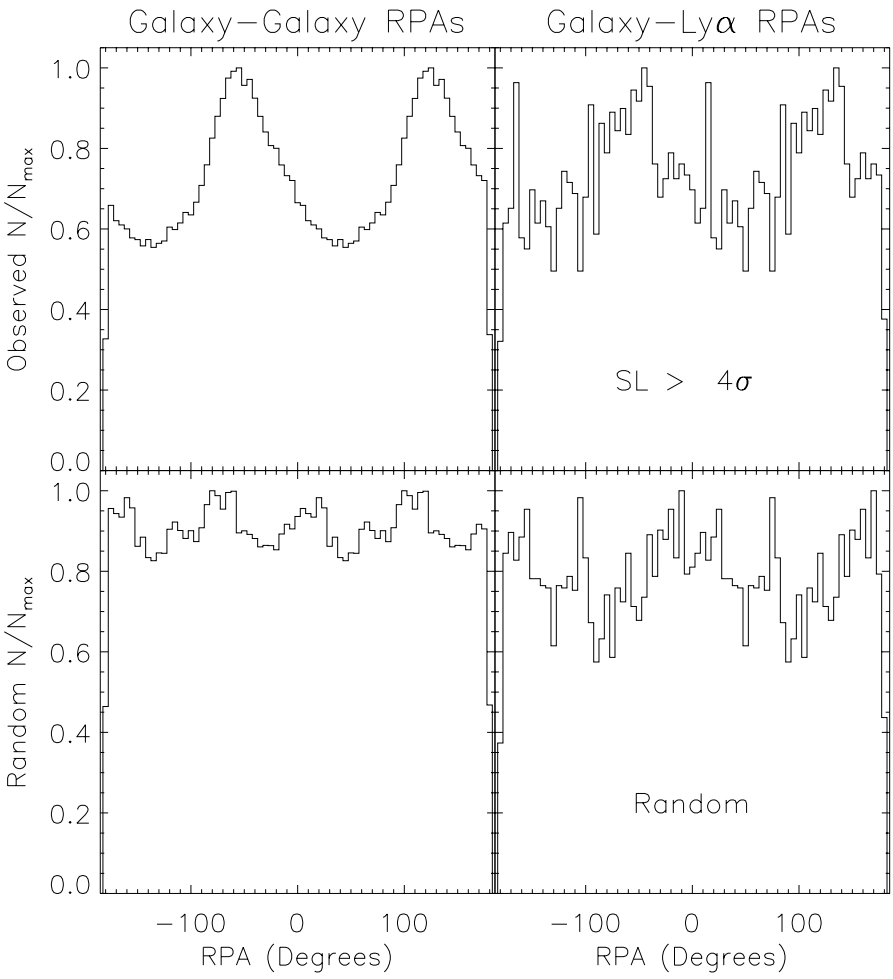

Fig. 9.— "Raw" galaxy-galaxy (left column) and absorber-galaxy (right column) position angles (PAs) using the spherical volume sampling described in the text, with Δv=450 km s^{-1} and an additional $\pm$150 km s^{-1} peculiar velocity. These PAs are "raw" in the sense that they have not been zero-pointed to the dominant PA of the galaxy distribution in each volume. The upper two panels correspond to our $SL \geq 4\sigma$ Lyα sample, while the lower panels refer to a random distribution. The large feature in the "raw" distributions at -55° and +125° is the "Great Wall", through which many of our sightlines pass.

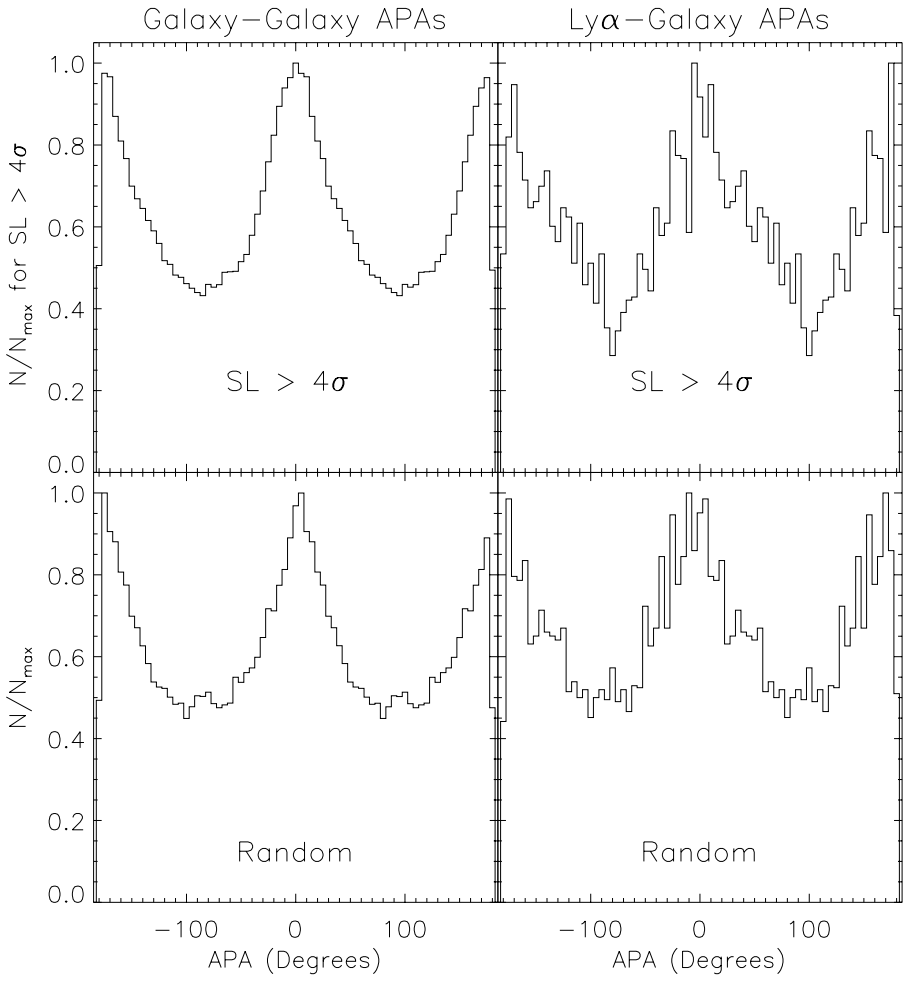

Fig. 10.— Aligned galaxy-galaxy (left column) and absorber-galaxy (right column) position angles (APAs) using the spherical volume sampling described in the text, with Δv=450 km s^{-1} and PV = $\pm$150 km s^{-1} peculiar velocity. The upper two panels correspond to our $SL \geq 4\sigma$ Lyα sample, while the lower panels refer to a simulated random distribution of absorber locations. Since these PAs have been adjusted to a zero point corresponding to the dominant PA of galaxy-galaxy vectors in each volume, the large peaks in these distributions indicate the same strong filamentary structure in the galaxy distribution along our sightlines.

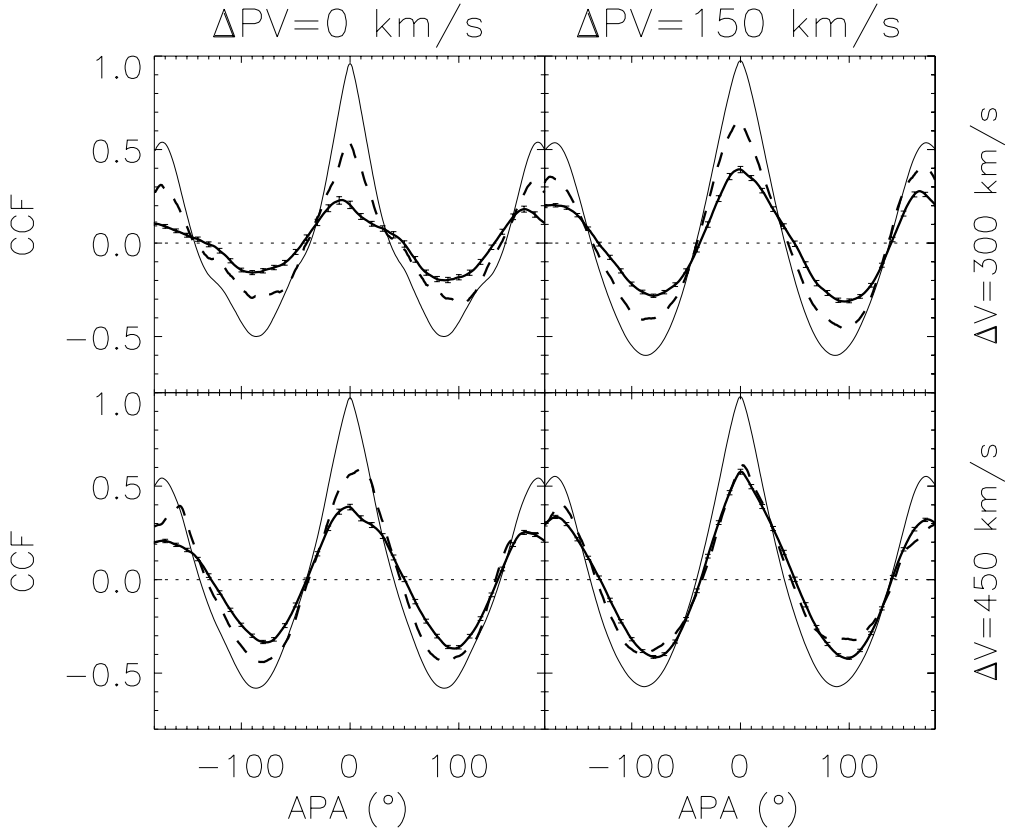

Fig. 11.— CCFs of the adjusted galaxy-galaxy (line solid line), absorber-galaxy (dashed line) and random absorber-galaxy (heavy solid line with 1σ error bars) position angles (APAs) using the spherical volume sampling described in the text. The upper panels show the CCFs for Δv=300 km s^{-1} ($4.3h_{70}^{-1}$ Mpc) and 0 km s^{-1} (left) and $\pm$150 km s^{-1} (right) peculiar velocity (PV) allowances. The bottom panels correspond to Δv=450 km s^{-1} ($6.4h_{70}^{-1}$ Mpc). The random absorbers in this figure were constructed using our "all-sky" method (see text). The detected absorber significance levels above the random distributions for each trial are given in Table 5.

5. $d\mathcal{N}/dz$ of Lyα absorbers in Voids

In this section, we explore the line-of-sight frequency $d\mathcal{N}/dz$ as a function of $\mathcal{W}$ for the low-z Lyα forest divided into void and "supercluster" subsamples. As before, we use only our $4\sigma L^*$ sample and define a void location as a region of space with no known galaxy within $3h_{70}^{-1}$ Mpc. We have explored using other methods to define voids along our sightlines, guided by the Slezak et al. (1993) wavelet transform method for defining voids in the original CfA survey. Since several of our GHRS sightlines pass through this region, we have used the Slezak et al. (1993) void boundaries to determine that a ± 300 km s^{-1} allowance from the edges of the supercluster filaments as defined by galaxy locations is an adequate representation of the void boundaries along our sightlines. Alternatively, ± 1000 km s^{-1} from the filament center is a slightly more conservative definition of the void boundaries (it yields slightly smaller voids than the first two definitions). The results stated below are for the simple $3h_{70}^{-1}$ Mpc definition, but all three definitions give the same result within the errors.

As in Paper II, we take $d\mathcal{N}/dz$ ($\mathcal{W} > \mathcal{W}_i$) to be the integrated line-of-sight frequency,

$$d\mathcal{N}/dz\ (\mathcal{W}\ > \mathcal{W}_i) = \int_{\mathcal{W}_i}^{\infty} \frac{\partial^2 \mathcal{N}}{\partial z\ \partial \mathcal{W}}\ d\mathcal{W}\ . \tag{1}$$

The upper panel of Figure 12 shows $d\mathcal{N}/dz$ ($\mathcal{W} > \mathcal{W}_i$) for our $4\sigma L^*$ void absorber sample as the solid line, while the supercluster $4\sigma L^*$ sample is shown by the dashed line. The $\mathcal{W}_i$ bins in this figure are 1 mÅ in width, and 1σ error bars are given every 20 $\mathcal{W}_i$ bins. Given the current limited sample, the ratio of $d\mathcal{N}/dz$ in superclusters to voids is consistent with a constant value of 3.8 ± 1.3 for all $\mathcal{W}$. In other words, $22 \pm 8\%$ of the low-z Lyα population are "void" absorbers. At this time, there is no statistically significant evidence that void and supercluster absorbers have different column density distributions, given that there are only 8 "void" absorbers in our sample. However, as can be seen in the bottom panel of Figure 12, which displays $d\mathcal{N}/dz$(void) divided by $d\mathcal{N}/dz$(SC=supercluster), there may be a slight overabundance of low $\mathcal{W}$ absorbers in "voids'. This is consistent with our earlier assertions (§ 3.2) that the low $\mathcal{W}$ absorbers showed a more random distribution.

We now follow the methodology given in Paper II for determining the cosmic baryon density, Ω_b. In Paper II we estimated that $\sim 20\%$ of the local baryonic matter may reside in these Lyα absorption systems. The relative number density of Lyα absorbers in voids and in superclusters found herein allows a first determination of the baryon density in voids. In Paper II, we pointed out that for isothermal spherical Lyα clouds of characteristic radius, R_{cl},

$$\Omega_b \propto \phi_{cl} R_{cl}^3 \propto \quad (d\mathcal{N}/dz)\ R_{cl}, \tag{2}$$

where ϕ_{cl} is the space density of the Lyα absorbers. While this estimate is dependent upon

both the geometry of the absorbers and the intensity of the ionizing radiation impinging on these clouds (see Paper II and Shull et al. (1998) for details), these factors enter here only if they are different for "void absorbers" compared to "supercluster absorbers". Thus, by assuming these factors are the same in voids and superclusters, the ratio of baryon density in clusters to that in voids is given by,

$$\frac{\Omega_b(\mathrm{void})}{\Omega_b(\mathrm{total})} = \frac{d\mathcal{N}/dz(\mathrm{void})}{d\mathcal{N}/dz(\mathrm{total})} \quad \left\langle \frac{R_{\mathrm{void}}}{R_{\mathrm{total}}} \right\rangle = 4.5 \pm 1.5\% \ \left\langle \frac{R_{\mathrm{void}}}{R_{\mathrm{total}}} \right\rangle . \tag{3}$$

Recent galaxy-void surveys have failed to turn up significant number of galaxies in voids down to impressively low luminosity limits (**?**, e.g., $\mathrm{M}_B \leq -13$;)]McLin02,Hibbard02. Therefore, since Lyα clouds are the only detectable baryons in voids, $4.5 \pm 1.5\%$ of the total baryonic density in the local Universe, inferred upon primordial nucleosynthesis, is contained in voids.

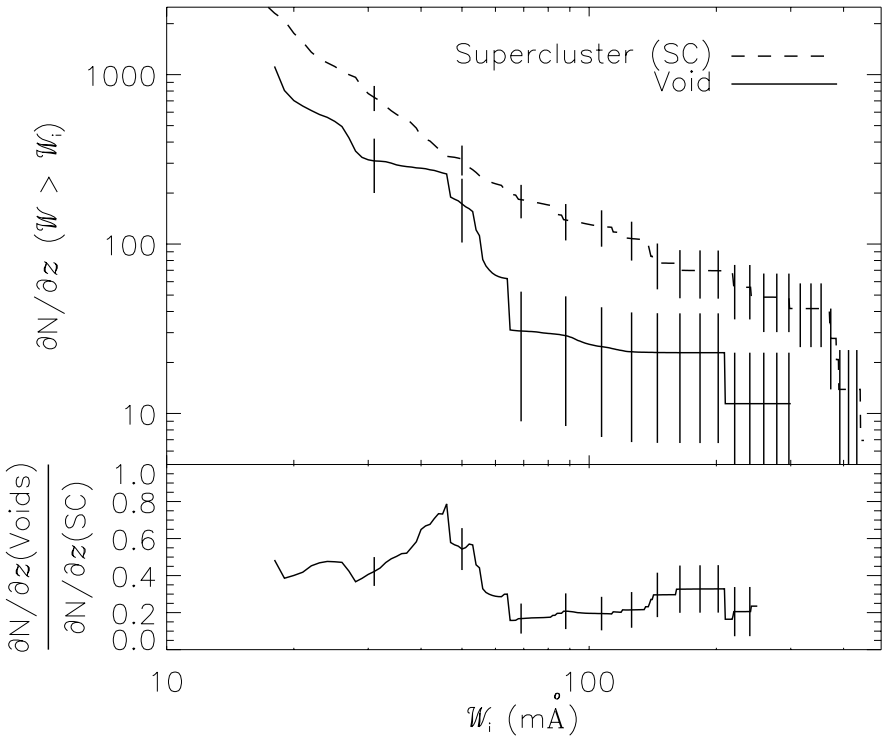

Fig. 12.— The upper panel displays the $d\mathcal{N}/dz$ spectrum in $\mathcal{W}$ of Lyα absorbers divided according to nearest-neighbor distance. The solid line in the upper panel gives $d\mathcal{N}/dz$ for our $4\sigma L^*$ void absorber sample, using a "void" nearest-neighbor limit of $3h_{70}^{-1}$ Mpc. Absorbers and regions of space not in voids are labeled as supercluster (SC), and $d\mathcal{N}/dz$ for these absorbers/locations are indicated by the dashed line. Error bars (1σ) are displayed for every 20 bins of 1 mÅ width. The bottom panel shows $d\mathcal{N}/dz$(voids) divided by $d\mathcal{N}/dz$(SC). This ratio suggests that the "void absorbers" may be of systematically lower $\mathcal{W}$ than the "supercluster absorbers". However, there are only 8 "void" absorbers in our sample, an insufficient number to make any statistically significant assertions.

6. Two Point Correlation Functions of Galaxy Halos and Lyα Absorbers

In this section, we determine the characteristic width of low-z galaxy filaments and voids, and compare the galaxy-galaxy two-point correlation function (TPCF) to the Lyα cloud TPCF determined in Paper II. Along each sightline, we extracted a cylindrical "core sample" through the CfA survey volume of galaxies with radii of 0.5, 0.75, and 1 h_{70}^{-1} Mpc. The 1D TPCF of the galaxies within these cylinders was determined using the location along the sightline of closest approach to each galaxy. Therefore, this is a measure of the TPCF of extended gaseous halos along these sightlines. As in the previous sections, to ensure approximately uniform galaxy information, we restrict our sightlines to our $4\sigma L^*$ sample, and to be consistent with our previous TPCFs, we do not include separations $\leq$ 50 km s^{-1}. To obtain information about larger separations, we do not restrict our pathlength to the available GHRS spectral coverage. We use the full "core sample" from a minimum cz=575 km s^{-1} to (cz_{em}– 1,200 km s^{-1}) from the target, provided that the sightline is still in a region of the CfA survey which is complete down to at least L^*. As in Paper II, we normalize by the expected random distribution to obtain the TPCF, $\xi(\Delta v) = N_{obs}(\Delta v)/N_{ran}(\Delta v) - 1$. For all trials, we see strong galaxy clustering below 2000 km s^{-1}, peaking at 10σ in the lowest separations. The TPCF for the $750h_{70}^{-1}$ kpc radius trial is displayed in Figure 13 and is quite similar to the other trials.

As is obvious in Figure 13, the galaxy-galaxy TPCF differs significantly from the Lyα TPCF and indicates that Lyα absorbers cluster nowhere near as strongly as galaxy halos would cluster along these sightlines. Within $\sim$750 km s^{-1}, the galaxy-galaxy TPCF has dropped to half of its peak value at the lowest separations. This leads us to the conclusion that the galaxy filaments in our sample are of order 750 km s^{-1} in velocity width, or $\sim 11h_{70}^{-1}$ Mpc. Peculiar velocities (PVs) would broaden the measured galaxy TPCF, so this estimate of low-z filament width is an upper limit. If we assume a PV of $\pm$ 200 km s^{-1} for galaxies in these filaments, then the actual physical width is $\sim 5h_{70}^{-1}$ Mpc. Therefore, the filaments are either rather broad, or the peculiar velocities within the filaments are large. This result is consistent with the filament widths found in § 4.2.

While the secondary peak at $\sim$ 8000 km s^{-1} in the galaxy TPCF is exactly the signal predicted by De Lapparent, Geller, & Huchra (1991) associated with galaxy voids of order 25-50 h_{70}^{-1} Mpc, we caution that the TPCF presented has insufficient pathlength per sightline to draw firm conclusions at $\Delta v > 3000$ km s^{-1}. The presence of Lyα clouds in voids is evidenced in Figure 13 by the rather uniform velocity distribution of Lyα absorbers compared to the deficiency in the galaxy-galaxy TPCF for $\Delta v \geq 1500$ km s^{-1}. Thus, the Lyα absorbers and galaxy halos cluster differently in two respects: (1) the Lyα absorbers do not exhibit the large clustering signature seen for the galaxy halos at $\Delta v < 1000$ km s^{-1} and (2) the Lyα absorbers

do not exhibit the TPCF deficiency beginning at $\Delta v \sim 1500$ km s^{-1} that occurs in the galaxy TPCF. Because the Lyα absorbers and galaxy halo TPCFs are significantly different (the K-S probability that they are drawn from the same parent population is $< 10^{-10}$), this gives additional support to the contention that these Lyα absorbers are not very extended galaxy halos. However, we caution that there has been a critique of the Lyα TPCF methodology by Fernandez-Soto et al. (1996) that claims that unresolved line blending in Lyα absorbers can hide significant clustering. Since higher resolution spectra (e.g., STIS echelle) show only modest line blending, and combined HST/FUSE Lyman line curve-of-growth analysis requires only 2–3 components per line to explain discrepancies in b-values (Shull et al. 2000), we suspect that effects of blending on the TPCF are small. Further, we see no way that this blending can produce a large TPCF excess at $\Delta v = 500 - 1000$ km s^{-1}, 10 to 20 times the velocity resolution of our data.

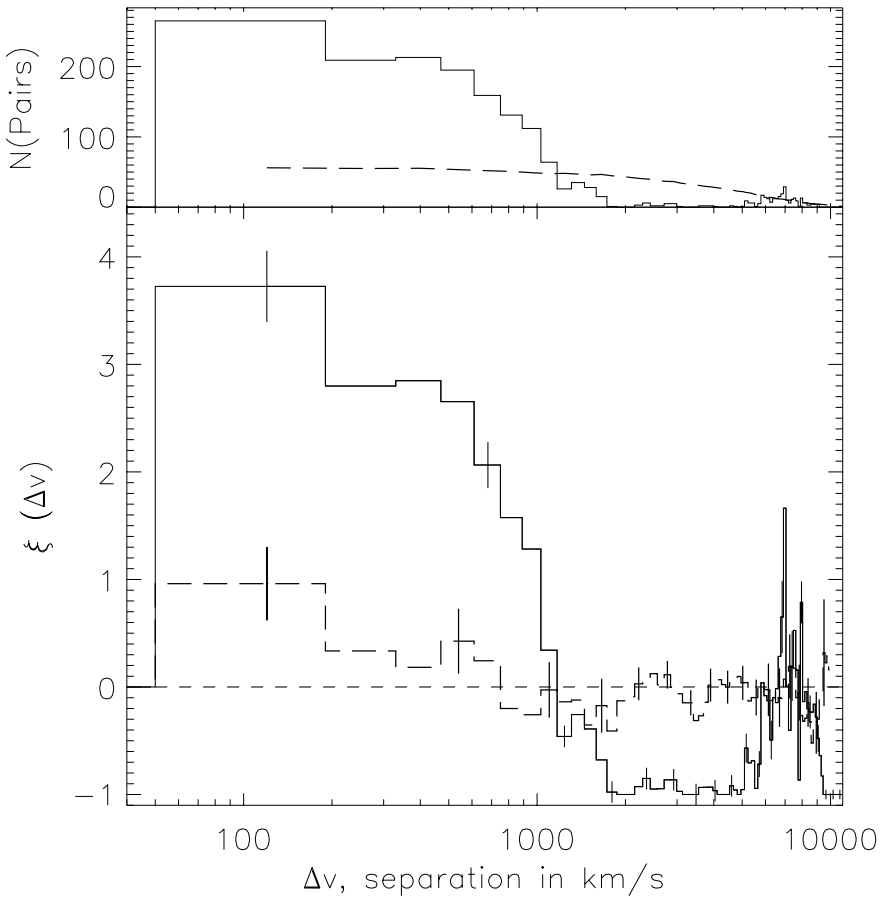

Fig. 13.— Galaxy-galaxy TPCF along our $4\sigma L^*$ sightlines with Δv = 140 km s^{-1} bins, including only galaxies within $750h_{70}^{-1}$ kpc of our HST sightlines. The upper panel compares the number, N(Δv), of galaxy pairs (solid histogram) to that expected for a random distribution (dashed line). The bottom panel compares the TPCF, $\xi(\Delta v)$, for galaxy halo pairs (solid histogram) to the TPCF for Lyα absorber pairs (dashed histogram). For clarity, we plot every fifth error bar and indicate the random TPCF (ξ=0) as a horizontal short-dashed line.

7. Conclusions

This paper is the third in a series whose purposes are to discover very low-z, low column density ($N_{\rm HI} \leq 10^{15}$ cm^{-2}) Lyα absorbers, determine their basic properties (e.g., line density, b-value distribution, TPCF amplitude, etc.), and determine their relationship with galaxies, voids, and large-scale structure in the local Universe. The papers in this series use Lyα detections made with the GHRS aboard the HST and utilized the G160M medium resolution first-order grating to obtain $\sim$ 19 km s^{-1} spectral resolution and limiting $\mathcal{W}$s as low as $\sim$ 12 mÅ. Future papers in this series will continue this investigation using newer spectra obtained with the Space Telescope Imaging Spectrograph (STIS) plus medium resolution gratings, which have similar spectral resolution and limiting $\mathcal{W}$ to the GHRS data.

In this paper we have used the Revised CfA Galaxy Redshift Catalog to compare the detected Lyα absorber locations to the actual galaxy distribution at low z. For the full sample, distances between Lyα absorbers and the nearest known CfA catalog galaxy neighbors range from $\sim 100h_{70}^{-1}$ kpc to $> 10h_{70}^{-1}$ Mpc. Because galaxy redshift information is non-uniform across the sky, we constructed a sub-sample of 46 $SL \geq 4\sigma$ Lyα absorbers. These absorbers are located in regions of the CfA catalog that have been completely surveyed down to at least L^* galaxies to achieve some level of consistency in the Lyα-galaxy correlation analysis. For the majority of our studies, we restrict ourselves to this $4\sigma L^*$ sample.

From the specific statistical results summarized below, we find no strong evidence that low column density, low-z Lyα absorbers arise in very extended galaxy halos. These absorbers may be a different population than some or all of the higher column density absorbers studied by L95 and C98. However, the absorbers do show a significant correlation with the large-scale distribution of galaxies. This conclusion is consistent with numerical simulations (**?**, e.g.,)]Dave99 of large-scale structure formation in which the low column density Lyα absorbers are true intergalactic material, not gas recycled by galaxies into the IGM. Observational work from several other groups (IPF99, Morris et al. 1993; Rauch et al. 1996; Tripp & Savage 1998, IPF99) support this interpretation. The results that draw us to this conclusion are:

- Of our 46 $4\sigma L^*$ HST/GHRS Lyα absorbers, 38 are within or near large-scale galaxy structures (filaments), while 8 are in galaxy voids. These percentages are similar, whether we use a nearest galaxy distance of $3h_{70}^{-1}$ Mpc, or the distribution of L^* galaxies to define the approximate regions of supercluster and void along our sightlines. Accounting for pathlength and sensitivity, we find that $22 \pm 8\%$ of low-z Lyα absorbers are in galaxy voids.

- While there are six absorber galaxy pairs in sufficiently close proximity ($\leq 230h_{70}^{-1}$ kpc)

to an L^* galaxy to be considered galaxy halos by previous work (L95, C98), the median distance between Lyα absorbers and galaxies in our $4\sigma L^*$ sample is $\sim 500 h_{70}^{-1}$ kpc, too large to be a plausible galaxy halo.

- In a cumulative nearest-neighbor distance distribution, our Lyα absorbers lie intermediate between random locations in space (median distance = $3 h_{70}^{-1}$ Mpc) and locations of galaxies (median distance to nearest galaxy = $250 h_{70}^{-1}$ Mpc). The median distance between Lyα absorbers and galaxies is $\sim 500 h_{70}^{-1}$ kpc, twice the median separation between bright galaxies. This is further evidence to doubt the association of Lyα clouds with individual galaxies. The strongest absorbers ($\mathcal{W} > 68$ mÅ) have nearest-galaxy distributions more similar to galaxies, while the weaker absorbers ($\mathcal{W} < 68$ mÅ) cluster more weakly. But the stronger absorbers still do not cluster as strongly as galaxies cluster (4σ difference). Although we have used different techniques for investigating the absorber-galaxy relationship, these results are similar to those recently reported by Tripp, Lu, & Savage (1998a) and IPF99.

- We find no correlation between Lyα absorber equivalent width and the sightline impact parameter with the nearest galaxy for low-$N_{\rm HI}$ absorbers, in contrast to the Lanzetta et al. (1995) and Chen et al. (1998) results at higher $N_{\rm HI}$. This lack of correlation is consistent with predictions of N-body+hydrodynamical simulations of the local Lyα forest (Davé et al. 1999), in which most absorbers and galaxies occupy the same large-scale structure filament. The L95 and C98 interpretation that Lyα absorbers are extended galaxy halos cannot be extrapolated to lower H I column densities and larger impact parameters than $\sim 250 h_{70}^{-1}$ kpc. Likewise, our interpretation that Lyα absorbers are intergalactic in nature cannot necessarily be extrapolated to the highest column densities and smallest impact parameters ($\leq 50 h_{70}^{-1}$ kpc).

- A detailed examination of the Q 1230+0115/3C 273 field for common absorbers, separated by only 0.9° on the sky ($230–550 h_{70}^{-1}$ kpc at $cz = 1000 - 2300$ km s^{-1}), is incompatible with a model in which spherical galaxy halos of high covering factor account for the observed Lyα absorbers. A possible filamentary gas structure $> 20 h_{70}^{-1}$ Mpc long can contain both galaxies and absorbers, and explains almost all the Lyα absorbers in this field. This example suggests that Lyα absorber studies combined with galaxy redshift surveys have the potential to map out local filamentary structure in both galaxies and gas (i.e., "cosmic tomography").

- We have compared statistically the location of Lyα absorbers relative to galaxies in known filamentary structures and find evidence, at the 5 to 12σ significance level, that Lyα absorbers are aligned with large-scale "filamentary" structures in the local Universe. This result reinforces our inference, based upon nearest-neighbor distances

that these Lyα absorbers are related to large-scale structure filaments, not individual galaxies.

- In Paper II we presented a two-point correlation function (TPCF) for Lyα absorber locations in the local Universe which found no excess power at $\Delta(cz) > 200$ km s^{-1} and a 4σ excess at $50 - 200$ km s^{-1}. Thus, local Lyα absorbers cluster together only very weakly, similiar to the clustering properties of Lyα absorbers at $z > 2$ (Rauch et al. 1992), and much less than galaxies cluster with each other. The difference between the clustering of galaxies and Lyα clouds was shown explicitly in this paper by constructing a TPCF of galaxy halos. The galaxy halo TPCF shows excess power at $\Delta v < 1000$ km s^{-1}, as well as a deficiency starting at $\Delta v \sim 1500$ km s^{-1}, which may be a signature of galaxy voids (De Lapparent, Geller, & Huchra 1991). The Lyα absorber TPCF shows neither of these signatures.

In Paper II we estimated that $\sim 20\%$ of the local baryonic matter may reside in Lyα absorption systems. Using the relative number density of Lyα absorbers in voids and in superclusters ($d\mathcal{N}/dz$(voids) is $22 \pm 8\%$ of $d\mathcal{N}/dz$(total)), allows a first determination of the baryon density in voids: $4.5 \pm 1.5\%$ of the total baryonic density inferred from primordial nucleosynthesis. This number should provide useful constraints on simulation of large-scale structure formation. Because these absorbers are the only detected material in voids, and because their total mean baryonic content (in both superclusters and voids) is comparable to that in galaxies, it is important to understand the details of their number density, physical conditions, metal abundance, and distribution in space relative to galaxies.

The HST/GHRS study presented in Papers I through III of this series have provided an important first step towards a detailed understanding of this important universal component. Future papers in this series will continue to refine the results herein by presenting: (1) updated statistical values (e.g., a revised TPCF) for low column density clouds based upon both the present dataset and spectra obtained with STIS/G140M (Penton, Stocke, & Shull 2002); (2) an updated analysis of the mean galaxy density surrounding local Lyα clouds similar to that conducted by Grogin & Geller (1998) but with many more absorbers (Grogin et al. 2002), and (3) deep galaxy surveys in regions surrounding the GHRS and STIS sightlines to determine if low luminosity and/or low surface brightness galaxies are responsible for Lyα absorptions, particularly the "void absorbers" (McLin et al. 2002; Hibbard et al. 2002).

The three papers in this series make up the bulk of the Ph.D. dissertation of S.V.P. at the University of Colorado, Boulder. For their assistance in obtaining the HST/GHRS data over several cycles, we are grateful to the staff at the Space Telescope Science Institute,

particularly Ray Lucas. We thank Mark Giroux for helpful discussions and a critical reading of the manuscript, and the referee, Chris Impey, for many helpful suggestions and criticisms. We also thank Jessica Rosenberg for her analysis of the Q1230+0115 STIS echelle spectrum. This work was supported by HST guest observer grant GO-06593.01-95A, by the HST/COS project (NAS5-98043), and by the Astrophysical Theory Program (NASA grant NAGW-766).

The Digitized Sky Surveys were produced at the Space Telescope Science Institute under U.S. Government grant NAG W-2166. The images of these surveys are based on photographic data obtained using the Oschin Schmidt Telescope on Palomar Mountain and the UK Schmidt Telescope. The plates were processed into the present compressed digital form with the permission of these institutions.

REFERENCES

Bahcall, J. N., et al. 1993, ApJS, 87, 1

Bowen, D. V., Blades, J. C., & Pettini, M. 1996, ApJ, 464, 141

Cen, R., Miralda-Escudé, J., Ostriker, J. P., & Rauch, M. 1994, ApJ, 437, L9

Chen, H.-W., Lanzetta, K. M., Webb, J. K., Barcons, X. 1998, ApJ, 498, 77 (C98)

Chen, H.-W., Lanzetta, K. M., Webb, J. K., Barcons, X. 2001, ApJ in press (astro/ph 0107137)

Cristiani et al. 1997, in Structure and Evolution of the IGM from QSO Absorption Lines, eds. P. Petitjean & S. Charlot, (Paris: Editions Frontières), 165

Davé, R., Hernquist, L., Katz, N., & Weinberg, D. 1999, ApJ, 511,521

De Lapparent, V., Geller, M. J., & Huchra, J. P. 1991, ApJ, 369, 273

Dinshaw, N., Foltz, C. B., Impey, C. D., Weymann, R. J., & Morris, S. L. 1995, Nature, 373, 223

Fernandez-Soto, A., Lanzetta, K.M., Barcons, X., Carswell, R.F., Webb, J.K. & Yahil, A. 1996 ApJ, 460, L85

Giovanelli, R., Williams, J. P., & Haynes, M. P. 1991, AJ, 101, 1242

Grogin, N. A., & Geller, M. J. 1998, ApJ, 505, 506 (GG98)

Grogin, N. A., Geller, M. J., & Huchra, J. P. 1998, ApJS, 119, 277 (GGH)

Grogin, N. A., Penton, S. V., & Stocke, J. T. 2002, in preparation

Hernquist, L., Katz, N., Weinberg, D. H., & Miralda-Escudé, J. 1996, ApJ, 457, L51

Hibbard, J. E., van Gorkom, J., Stocke, J. T., and McLin, K. 2002, in preparation

Hoffman, G. L., Lu, N. Y., Salpeter, E. E., Connell, B. M. and Fromhold-Treu, R. 1998, ApJ, 500, 789

Huchra, J., Geller, M., Clemens, C., Tokarz, S., & Michel, A. 1992, Bull. C.D.S., 41, 31

Huchra, J. P., Vogeley, M. S., & Geller, M. J. 1999, ApJS, 121, 287

Impey, C. D., 1997, in Structure and Evolution of the IGM from QSO Absorption Lines, eds. P. Petitjean & S. Charlot, (Paris: Editions Frontières), 101

Impey, C. & Bothun, G. 1997, ARA&A, 35, 267

Impey, C. D., Petry, C. E., & Flint, K. P. 1999, ApJ, 524, 536 (IPF99)

Jannuzi, B. T., et al. 1998, ApJS, 118, 1

Lanzetta, K. M., Bowen, D. V., Tytler, D., & Webb, J. K. 1995, ApJ, 442, 538 (L95)

Linder, S. M. 2000, ApJ, 529, 644

Marzke, R. O., Huchra, J. P., & Geller, M. J. 1994, ApJ, 428, 43

Marzke, R. O., Huchra, J. P., & Geller, M. J. 1996, AJ, 112, 1803

McLin K., Stocke, J. T., Weymann, R. J., Penton, S. V., & Shull, J. M., 2002, ApJ, in preparation

Mo, H. J. & Morris, S. L. 1994, MNRAS, 269, 52

Mo, H. J. & Mao, S. 2000, MNRAS, 318, 163

Morris, S. L., Weymann, R. J., Savage, B. D., & Gilliland, R. L. 1991, ApJ, 377, L21

Morris, S. L., Weymann, R. J., Dressler, A., McCarthy, P. J., Smith, B. A., Terrile, R. J., Giovanelli, R., & Irwin, M. 1993, ApJ, 419, 524

Morris, S. L., & van den Bergh, S. 1994, ApJ, 427, 696

Penton, S. V., Stocke, J. T., & Shull, J. M. 2000a, ApJS, 130, 121 (Paper I)

Penton, S. V., Shull, J. M., & Stocke, J. T. 2000b, ApJ, 544, 150 (Paper II)

Penton, S. V., Stocke, J. T., & Shull, J. M. 2002, in preparation (Paper IV)

Ramella, M., Geller, M. J., & Huchra, J. P. 1992, ApJ, 384, 396

Rauch, M., Carswell, R. F., Chaffee, F. H., Foltz, C. B., Webb, J. K., Weymann, R. J., Bechtold, J., & Green, R. F. 1992, ApJ, 390, 387

Rauch, M., Weymann, R. J., & Morris, S. L. 1996, ApJ, 458, 518

Salzer, J. J., di Serego Alighieri, S., Matteucci, F., Giovanelli, R., & Haynes, M. P. 1991, AJ, 101, 1258

Sargent, W. L. W. 1987 in QSO Absorption Lines, ed. J. C. Blades, D. Turnshek & C. A. Norman (Cambridge: Cambridge Univ. Press), 1.

Sembach, K. R, Howk, J. C., Savage, B. D., Shull, J. M., & Oegerle, W. R., 2001, ApJ, in press (astro-ph/0108047)

Shull, J. M., Stocke, J. T., & Penton, S. V. 1996, AJ, 111, 72

Shull, J. M. 1997, in Structure and Evolution of the IGM from QSO Absorption Lines, ed. P. Petitjean & S. Charlot, (Paris: Editions Frontières), 101

Shull, J. M., Penton, S. V., Stocke, J. T., Giroux, M. L., van Gorkom, J. H., Lee, Y. H., & Carilli, C. 1998, AJ, 116, 2094

Shull, J. M., Penton, S. V., & Stocke, J. T. 1999a, PASA, Vol. 16, No. 1, 95

Shull, J. M., Roberts, D., Giroux, M. L., Penton, S. V., & Fardal, M. A. 1999b, AJ, 118, 1450

Shull, J. M. et al. 2000, ApJ, 538, L13

Slezak, E., de Lapparent, V. & Bijaoui, A. 1993, ApJ, 409, 517

Songaila, A., & Cowie, L. L. 1995, AJ, 112, 335

Stocke, J. T., Shull, J. M., Penton, S. V., Donahue, M., & Carilli, C. 1995, ApJ, 451, 24

Tripp, T. M., Lu, L., & Savage, B. D. 1998a, ApJ, 508, 200

Tripp, T.M., Lu, L., & Savage, B. D. 1998b, in The Scientific Impact of the Goddard High Resolution Spectrograph, ASP Conference Series, Vol. 143, ed., J. C. Brandt, T. B. Ake, C. C. Peterson, 261

Tytler, D., Fan, X.-M., Burles, S., Cottrell, L, Davis, C., Kirkman, D., & Lin, Z. 1995, in QSO Absorption Lines, ed. G. Meylan (Berlin: Springer), 289

van Gorkom, J. H., Bahcall, J. N., Jannuzi, B. T., & Schneider, D. P. 1993, AJ, 106, 2213

van Gorkom, J. C., Carilli, C. L., Stocke, J. T., Perlman, E. S., & Shull, J. M. 1996, AJ, 112, 1397

Weymann, R. J., 1995, in QSO Absorption Lines, ed. G. Meylan (Berlin: Springer), 3

Weymann, R. J. et al. 1998, ApJ, 506, 1

Zhang, Y., Meiksin, A., Anninos, P., & Norman, M. 1997, ApJ, 495, 63

AAS LaTeX macros v5.0.